Karazin Kharkiv National University
Department of Physics and Technology

Technische Universität Darmstadt
Institut für Kernphysik

Remote Control Program for Target Positioning in the

Target Chamber of the Lintott Spectrometer

and

Test of Pseudospin Symmetry through ℓ-Forbidden

Gamow-Teller Transitions

Diploma Thesis

Anatoliy Byelikov

Darmstadt 2003

Abstract

The present diploma thesis consists of an experimental and a theoretical part. In the first one a Windows based program using the LabView software was developed and tested for the remote control of various gadgets located inside the target chamber of the Lintott spectrometer. The commands, generated by the program, are transmitted to the stepper motor control unit IXE which operates the corresponding devices. In particular, it allows to select the proper target and the according target position as well as to handle the target chamber light and the alignment laser. The entire system has passed successfully a long-term test. The corresponding program code is listed.

In the second part of the present diploma thesis nuclear matrix elements for the ℓ-forbidden Gamow-Teller transitions were calculated for different shells using pseudospin symmetry predictions. The results of these calculations were compared to experimental values. Reasonable agreement was found only for 2s-1d shell, while for the 2p-1f and 3s-2d-1g shells the agreement is unsatisfactory.

Анотація

Дипломна робота складається з експериментальної та теоретичної частин. У першій частині було розроблено та протестовано Windows-орієнтовану програму для керування різноманітними пристроями, що їх розміщено в камері розсіювання Lintott спектрометра. Команди, сгенеровані програмою, передаються до модулю керування поступовим двигуном, який приводить у дію належні пристрої. Цілковита система вдало подолала довготривалий тест. Належний програмний код наведено у додатку А.

У другій частині цієї дипломної роботи було розраховано матрічні елементи для заборонених по ℓ переходів Гамова-Телера, використовуючи предречення псевдоспінної симетрії, а також проведено порівняння їх із експериментально отриманими величинами. Прийнятне узгодження було винайдене для 2s-1d оболонки, у той час як для 2p-1f та 3s-2d-1g оболонок узгодження незадовільне.

Введение

Данная дипломная работа состоит из экспериментальной и теоретической частей. В первой части была разработана и протестирована программа для удалённого контроля различными устройствами внутри камеры рассеяния Lintott спектрометра. Команды, сгенерированные программой, передаются модулю управления шаговым двигателем, который приводит в действие нужные устройства. Целая система удачно преодолела долгосрочный тест. Соответствующий программный код можно найти в приложении А.

Во второй части этой работы были расчитаны матричные элементы для запрещённых по ℓ переходов Гамова-Теллера, используя предсказания псевдоспинной симметрии, а также проведено сравнение их с экспериментально измеренными величинами. Приемлемое соответствие найдено для 2s-1d оболочки, в то время как для 2p-1f и 3s-2d-1g оболочек соответствие неудовлетворительное.

Contents

Introduction

The investigation of nuclear structure with the help of inelastic electron scattering is the most important application of the superconducting Darmstadt electron linear accelerator S-DALINAC at the Institute of Nuclear Physics of the Darmstadt University of Technology. Due to its contemporary concept the S-DALINAC is a high quality source of a continuous electron beam with energies up to 130 MeV. For a momentum analysis of the scattered on the target electrons the so-called QCLAM spectrometer is used. With its large solid angle and momentum acceptance this spectrometer is well suited for (e,e′x) coincidence and 180° scattering experiments [1-3].

Additionally, a spectrometer for high resolution (e,e′) experiments that was previously used with the former normal-conducting accelerator DALINAC [4-7] is available. In order to carry out high resolution scattering experiments especially with heavy nuclei, where the level densities are high, a new detector system is presently developed for the spectrometer [8].

It is necessary for users to be able to select different targets during the experiment without entering the experimental hall. One target may serve for calibration and others for measurements. A stepper motor can be used for this purpose. The development of a Windows based program for controlling the target position and some other relevant actions is the aim of the first part of the present diploma thesis.

The second part deals with the phenomenon of pseudospin symmetry in nuclei. Pseudospin symmetry is a quasidegeneracy of spin levels with quantum numbers (*n, l, j=l+1/2*) and (*n-1, l+2, j=l+3/2*). Recently a new interpretation of pseudospin symmetry has been given [9] to result from a SU(2) symmetry of the Dirac Hamiltonian. Assuming this, specific predictions can be made for transitions between pseudospin partners. The aim of the second part of the diploma thesis was to perform an analysis of the theoretical predictions for Gamow-Teller transitions using available experimental data from ground state β-decay.

Experimental set-up

1.1. S-DALINAC and its experimental facilities

The S-DALINAC was constructed in the Institute of Nuclear Physics of the Darmstadt University of Technology [10]. It became the first superconducting continuous-wave linear accelerator of electrons in Europe. Since 1991 the S-DALINAC delivers electron beams with a maximum energy of 130 MeV and currents of up to 60 μA for a wide range of experiments. The layout of the S-DALINAC is shown in fig. 1.
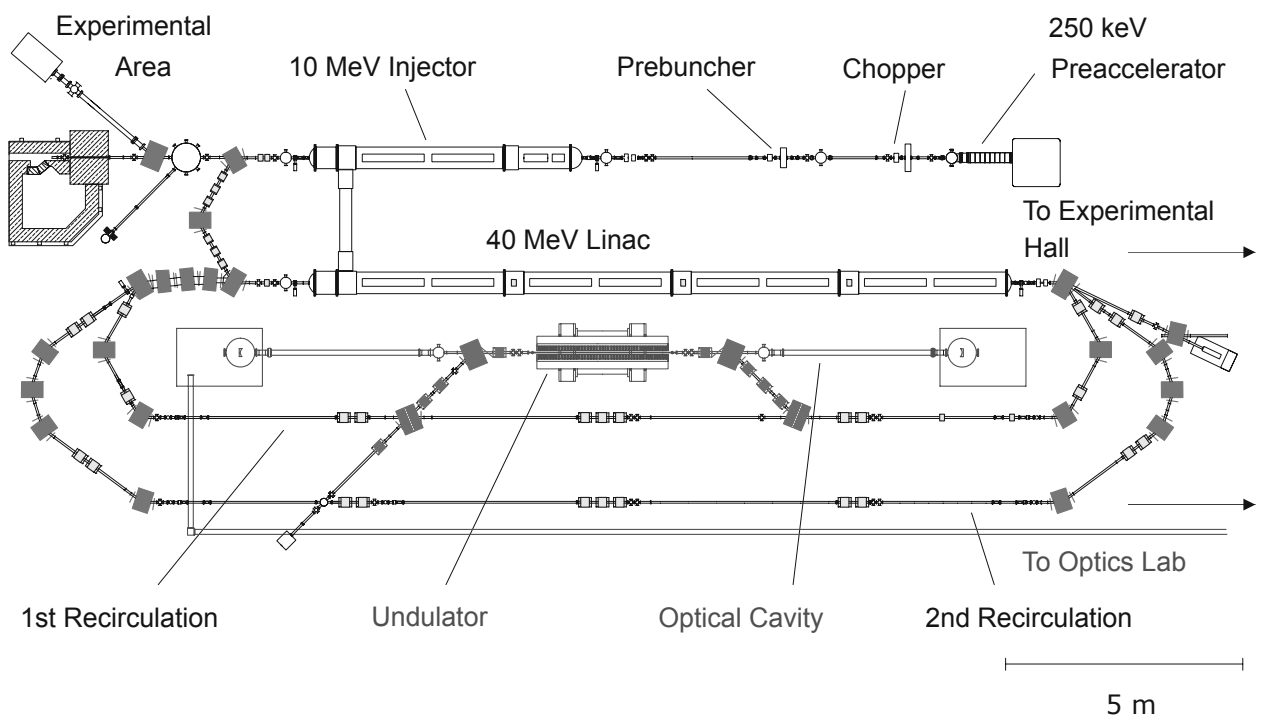
Fig. 1: Schematic layout of the S-DALINAC.

The electrons are emitted by a thermionic gun and then accelerated electrostatically to an energy of 250 keV. The required time structure of the electron beam for radio-frequency acceleration in a 3 GHz field is created by a chopper/prebuncher system operating at room temperature. The superconducting injector linac consists of one 2-cell, one 5-cell, and two standard 20-cell niobium cavities cooled to 2 K by liquid helium. The beam leaving the injector has an energy up to 10 MeV and can either be used for radiation physics experiments or for nuclear resonance fluorescence experiments. Alternatively, it can be bent by

8

180^0 and injected into the main accelerator section. This superconducting linac has eight 20-cell cavities which provide an energy gain up to 40 MeV. After passing through the main linac the electron beam can be extracted to the experimental hall or it can be recirculated and reinjected one or two times. Additionally, in the first recirculation beam-line an infrared Free Electron Laser (FEL) is located. The electron beam with a maximum energy of up to 130 MeV is delivered to several experimental facilities, shown schematically in fig. 2.
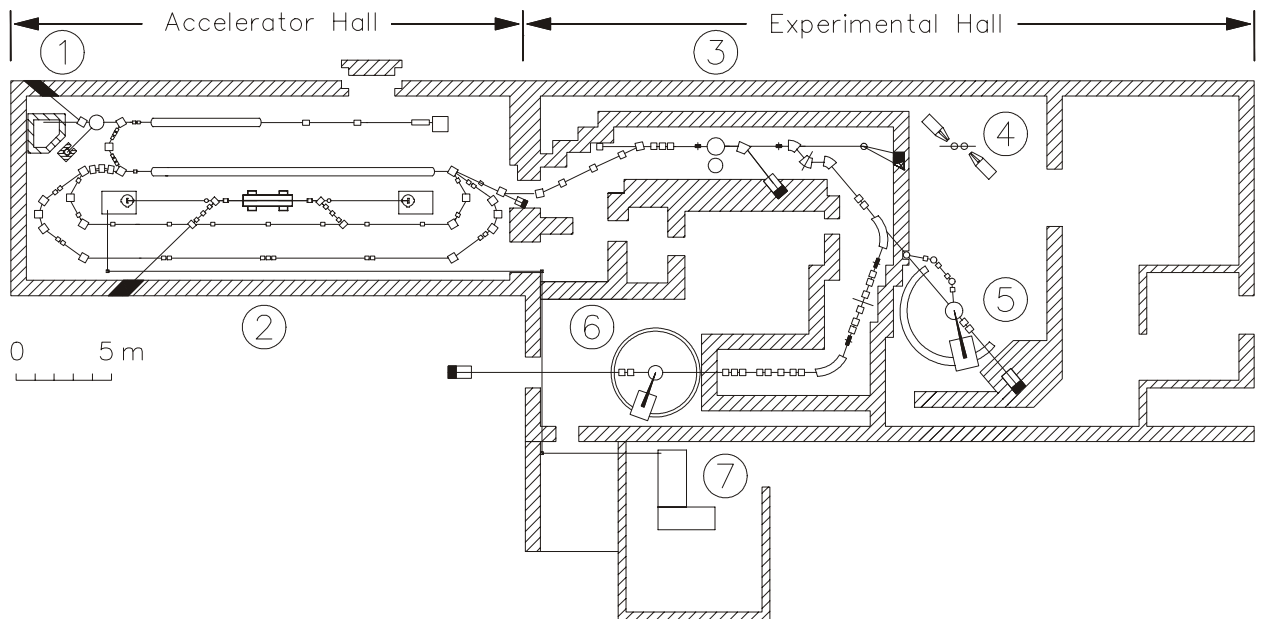
Fig. 2: Experimental facilities at the S-DALINAC.

① channeling radiation and (γ,γ') experiments, ② Free Electron Laser, ③ high energy radiation physics, ④ high energy bremsstrahlung experiments ⑤ (e,e') at 180° and (e,e'x) experiments, ⑥ (e,e')-experiments, ⑦ optic experiments.

A wide range of electron scattering experiments is carried out using the QCLAM spectrometer (Pos. 5) and a high resolution energy-loss facility with a Lintott spectrometer (Pos. 6). The Lintott spectrometer operates in the so-called "energy-loss" mode that enables to perform high resolution (e,e') experiments independently of the energy spread of the electron beam [5].

1.2. High resolution energy-loss system

The layout of the high resolution energy-loss system is shown in fig. 3. This system provides the operation of the spectrometer in the so-called energy-loss mode.
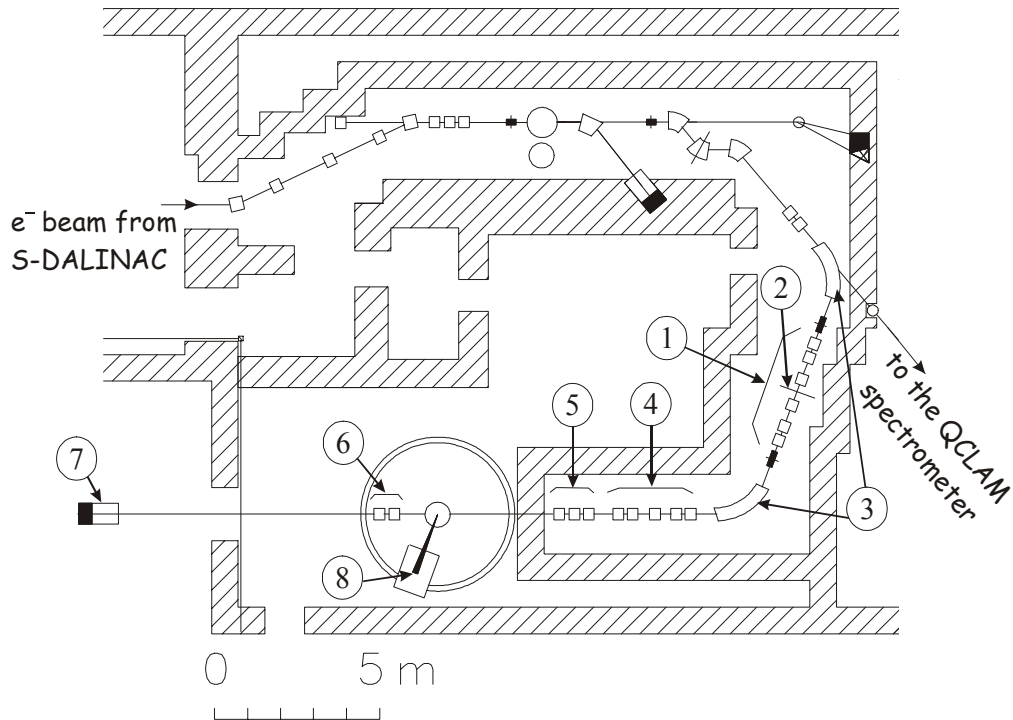
Fig. 3: High resolution energy-loss system.
① focusing quadrupoles, ② energy defining slit, ③ 70° bending magnets, ④ "rotator", ⑤ focusing quadrupole triplet, ⑥ refocusing quadrupole doublet, ⑦ Faraday cup, ⑧ energy-loss spectrometer.

The system consists of six quadrupoles (Pos. 1) and two 70° bending magnets (Pos. 2) which form a momentum analyzing system with energy defining slits (Pos. 3) in the symmetry plane between these magnets. A set of five quadrupoles called "rotator" (Pos. 4) is used to turn the dispersion plane at 90° in the energy-loss mode of operation, and the quadrupole triplet (Pos. 5) focuses the beam onto the target. A quadrupole doublet (Pos. 6) behind the target reduces the beam divergence due to multiple scattering and delivers it to a Faraday cup (Pos. 7) that simultaneously serves as a monitor of the current. The scattered electrons are analyzed by the Lintott spectrometer (Pos. 8).

The Lintott spectrometer is shown in fig. 4. The electron beam from the accelerator hits the target which is placed inside the scattering chamber at the pivot-point of the spectrometer (Pos. 1). The scattered electrons pass the spectrometer entrance slit defining the accepted solid angle Ω, and are deflected by the dipole magnet (Pos. 2) to an angle of $\pi\sqrt{8/3} = 169.7°$ (this angle is called "magic"). Then the electrons exit through the output vacuum chamber (Pos. 4) and are focused onto the focal plane.
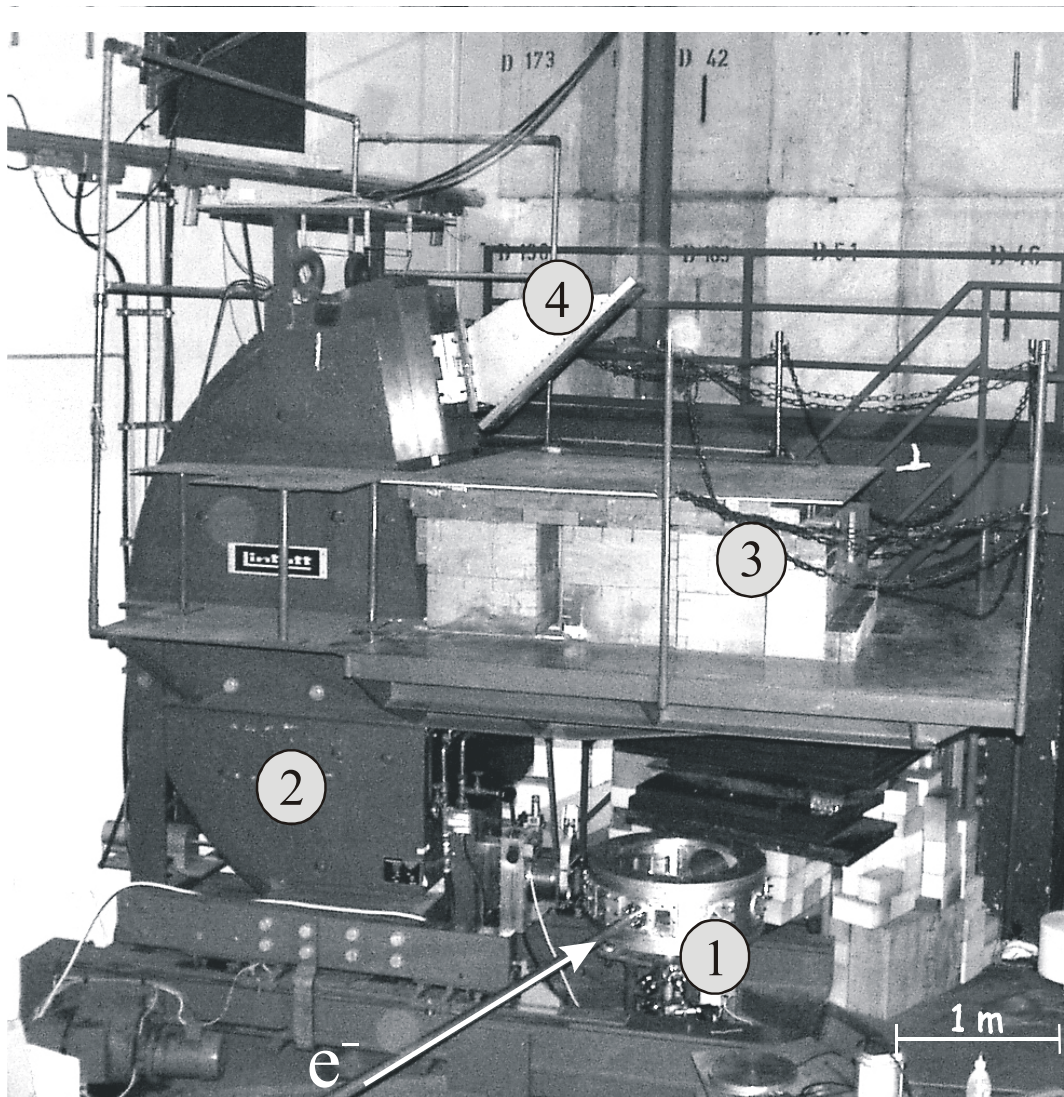
Fig. 4: The Lintott spectrometer without detector system.
① target chamber, ② dipole magnet, ③ paraffin and lead shielding, ④ vacuum chamber.

1.3. Target chamber

In fig. 5 an internal view of the target chamber is shown. The incoming electrons (Pos. 1) scatter at the main target (Pos. 4) and then exit from the target chamber through the slit to the dipole magnet of the Lintott spectrometer (Pos. 7).
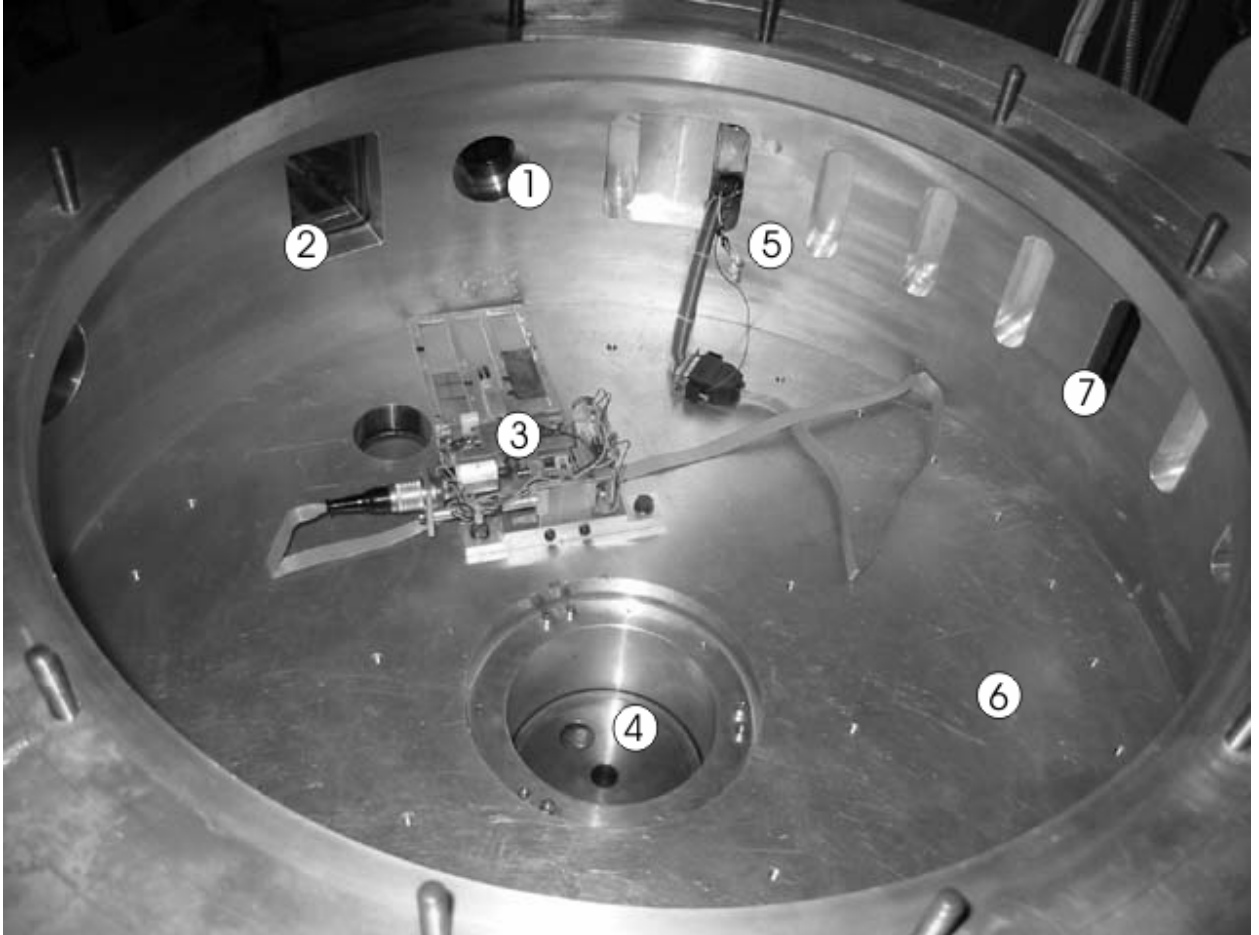
Fig. 5: Target chamber.

① incoming electron beam/laser beam, ② window for TV camera, ③ flip-target, ④ main target holder place, ⑤ light source, ⑥ construction elements, ⑦ exit slit for the scattered electrons into spectrometer

A flip-target and a laser are used for the beam position calibration. For better experimental results it is important that the electrons hit the target exactly in the center. This can be achieved by the following steps:

- First the flip-target is moved up and the user registers the position, where the laser beam hits the target.
- Then the flip-target is moved down and the user has to adjust the main target in such a way that the registered laser beam spot can be correlated with the

position recorded on the flip-target. After this procedure the flip- and main targets are correlated with respect their disposition.

- Then the flip-target is moved up again, the laser is turned off and the electron beam hits the target. The system is organised so that the electron beam is parallel to the laser beam. The flip-target emits light when electrons hit it, the main target, as a rule, not. Once these targets are correlated the user can adjust the beam to hit flip-target in the center assuming that the electron beam will hit the main target also in the center when the flip-target is down.

One should remark that the magnets, adjusting the electron beam (fig. 3), are so far away from the target chamber that their field does not affect the electrons inside.

1.4. Required features of the target control program

Now one can specify the tasks that a program must be able to do.

- Move the main target placed on the platform up and down to definite positions.
- Flip the flip-target up and down and, when it is in the up position, also left and right.
- Turn the laser on and off.
- Turn the light on and off.
- The current position of the main target and current state of the flip-target, laser and light should be indicated.

2. Stepper motor control unit

All the necessary actions specified in chapter 1.4. are performed by a stepper motor control unit. The present program has been written and tested with the IXEα-C-RS motor control unit (further IXE) belonging to the stepper motor ZSS52-200-2.5. In the standard version IXE is equipped with a RS-232 serial computer interface, 12 input connectors and 8 output ones. The program, however, controls only 7 inputs and 4 outputs, that are used.

2.1. ZSS-series stepper motor

For moving the main target up and down a ZSS52-200-2.5 stepper motor is used. The platform has a diameter of 52 mm, it makes 200 steps per revolution and has a winding of 2.5 mm. A schematic view of the motor (target lift) is shown in fig. 6.
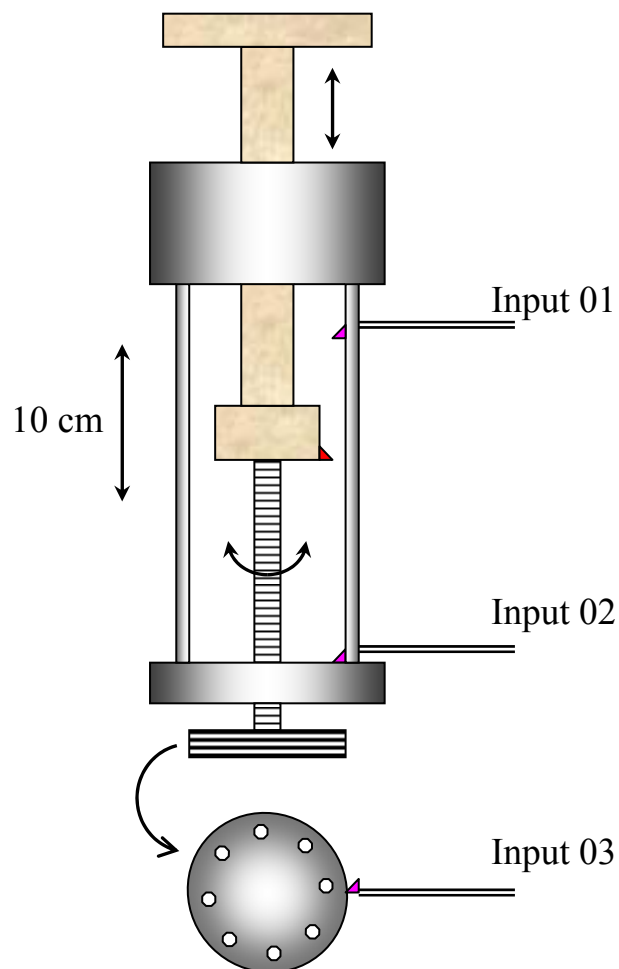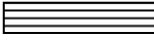
Fig. 6: Scheme of the stepper motor.

- non-movable part
- rotating part
- linear moving part
○ - magnets on the rotating ring
- magnet on the linear moving rod
- trigger detectors

14

When the linear moving part reaches the top or bottom position, a magnet fixed on it is directly opposite to the magnet of one of the detecting triggers, which are connected to the IXE inputs 01 (top) & 02 (bottom). A trigger turns to the OFF position and sends a logical "false" signal to the corresponding input.

The same holds for input 03. If one of the eight magnets situated on the rotating ring appears opposite to the detecting trigger, it turns it to the OFF position. The detecting trigger of input 03 is used to control whether the motor is moving or not. If a signal on it changes then the motor is moving. Such a system is called ticker.

2.2. IXE inputs

As described above, input 01 is responsible for the registration of the top position state, input 02 – for that of the bottom position and input 03 for the signal from the ticker. The remaining four inputs (04, 05, 06 and 07) are responsible for controlling the flip-target position. Table 1 shows all possible variants of the states of these inputs.

Table 1: Description of the possible states of the flip-target

Input 04	Input 05	Input 06	Input 07	Description
OFF	ON	OFF	OFF	Flip-target is in down position
ON	ON	OFF	OFF	Flip-target is moving up or down
ON	OFF	OFF	ON	Flip-target is in the up normal position
ON	OFF	ON	OFF	Flip-target is in the up reverse position

2.3. IXE outputs

The stepper motor control unit has 8 outputs that can be programmed to 1 or 0 by the user. The program controls four of these outputs. Output 1 is used for moving flip-target up and down. Output 2 rotates the flip-target, when it is up, to normal or reverse to the beam position. Output 3 turns the light on and off. Output 4 performs the same to output 3 with the laser.

3. The LabView control program

3.1. Program features

The control program was realised using LabView software. It was elaborated and tested on the PC system based on the Intel© Pentium™ 133 MHz processor with 32 Mb random access memory. For the proper operation the program requires the preinstalled National Instruments LabView application.

The front panel of the program is designed for the screen resolution of 1024x768 pixel with a 16 bit colour depth.

The program works correctly with the stepper motor operating in the ministep mode with a ministep factor of 10, i.e. 10 steps correspond to 1 motor step. In other words, 200 steps per revolution of the motor become 2000 steps per revolution in the computer programming mode. It is important to note that in the full step, half step or ministep mode different from 10 this program will not work correctly. The ministep mode is determined by the position of a switch inside the stepper motor control unit. It can not be selected or read by a program.

3.2. Program front panel

The view of the program control panel is shown in fig. 7. It consists of the following elements.

1. VISA resource name. It determines to which computer port the IXE unit is attached. The default value is COM1.
2. Axis pull down menu. It indicates the name of the axis to operate with.
3. Frequency pull down menu. It selects the operating frequency.
4. Initialize IXE button. It is used for accepting the chosen values.
5. Inputs state indicators. They show the current state of the inputs 04, 05, 06, 07.
6. Error indicator. If an error occurs during the program execution this indicator lights up.
7. Current position indicator. It shows the current position of the main target holder.
8. Digital display for current position indicator.

16

9. Busy indicator. It lights up when the stepper motor is moving.

10. Top position indicator. It lights up when the main target is in the top position.

11. Bottom position indicator. It lights up when the main target is in the bottom position.

12. Flip target u/d button. It is used to flip the flip-target in the up or down position.

13. Flip target u/d indicator. When it is "off" then target is down, when "on" – target is up.

14. Flip target l/r button. When the flip-target is up pressing this button flips it to the normal or reverse to the beam position.

15. Flip target l/r indicator. When it is "off" the flip-target is in normal position, when "on" – in reverse position.

16. Light on/off button.

17. Light indicator.

18. Laser on/off button.

19. Laser indicator.

20. Dial, which is used to select the value of the distance to move. Distance is given in mm.

21. Digital control for the dial 20 of this list.

22. Switch, that selects a direction to move. The direction can be either positive (up) or negative (down).

23. Go button. After pressed, the motor moves the main target on the value of the distance, selected by controls 20-21 of this list, in the direction selected by switch 22 of this list.

24. End button: when pressed, program ends execution.
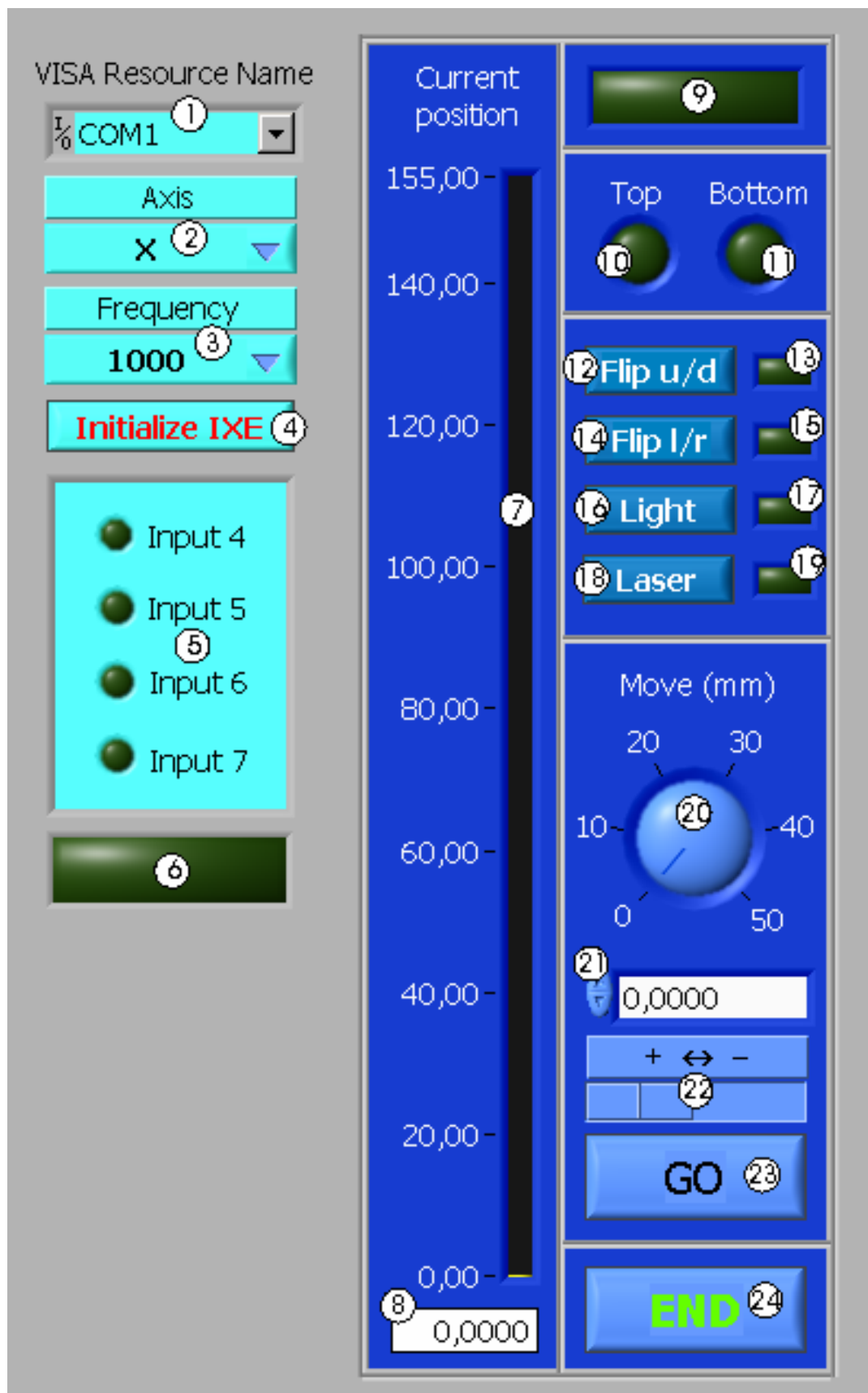
Fig. 7: View of the front panel of the program. The description of the elements is given in the text in chapter 3.2.

3.3. Visual operation

After the start the program is in an initialization waiting mode. The user has to select the port (Pos. 1 in fig. 7) to which IXE is connected, the working axis (Pos. 2) and the frequency (Pos. 3). Then the button "Initialize IXE" (Pos. 4) needs to be pushed.

If the settings are correct the program turns off the chamber light and the laser, moves the flip-target down and the main target into its bottom position. The busy indicator (Pos. 9) is on during this performance.

Afterwards the front panel must have the following appearance. The state indicator of input 5 (Pos. 5) and bottom position indicator (Pos. 11) should be "on", all others "off". The indicator of the current position of the main target (Pos. 7-8) must show "0.0000".

Thereafter the program is ready to perform any relevant settings such as turning light and laser on and off, moving the flip-target up-down and left-right, moving the main target up-down on any value within the limits of the work zone between the bottom and top positions.

In order to finish the program the end button (Pos. 24) needs to be pushed. The program closes the connection between IXE and PC and terminates.

3.4. Program internal organization

The program consists of five successive parts. They are: initialization, activation, calibration, work and deactivation. The first three are preparatory parts, the last one is conclusive part. The main part that corresponds to the visual operation with the front panel is the work part. The detailed overview of all these parts and their LabView code is given in appendix A.

3.5. Conclusion

Finally, the program, written within the frame of the present thesis, fulfills all the requirements, listed in chapter 1.4. It has a convenient user interface and handles the errors, which can appear during its performance. The program was

tested during several months under realistic conditions. It worked without problems and executed all functions successfully.

4. Test of pseudospin symmetry through ℓ-forbidden Gamow-Teller transitions

4.1. Pseudospin symmetry and ℓ-forbidden transitions

The idea of pseudospin was introduced to explain the quasidegeneracy in spherical nuclei between single-nucleon states with quantum numbers (*n, l, j=l+1/2*) and (*n-1, l+2, j=l+3/2*), where *n, l* and *j* are the radial, the orbital and the total angular momentum quantum numbers, respectively. Nuclei showing this behavior appear throughout the whole nuclear landscape. Such a degeneracy was also observed between Nilsson states in deformed nuclei.

This doublet structure can be expressed in terms of a "pseudo-orbital" angular momentum quantum number $\tilde{l} = l + 1$, where the two levels represent spin-orbit partners with a "pseudospin" quantum number $\tilde{s} = 1/2$. While this concept of a pseudospin symmetry was empirically established 30 years ago [11,12], a deeper understanding has been lacking. Only recently the subject was revived when Ginocchio [13] recognized, for the first time, the relativistic character of the symmetry. He noted that the pseudo-orbital angular momentum is just the orbital angular momentum of the lower component of the Dirac spinor. He also showed that pseudospin symmetry is an exact symmetry for the Dirac Hamiltonian with an attractive scalar potential S and a repulsive vector potential V, when they are equal in magnitude: $S + V = 0$. It turns out that this symmetry is nothing but a SU(2) symmetry of the Dirac Hamiltonian [14].

Transitions between pseudospin partners are of so-called ℓ-forbidden M1 type. The term "ℓ-forbidden" refers to a selection rule of the unrenormalized one-body magnetic dipole operator which does not permit a change of the radial quantum number. The description of M1 and the closely related Gamow-Teller (further GT) transitions requires modifications of the bare one-body operators to describe the phenomenon of spin quenching in nuclei [15].

In allowed M1 and GT transitions, the weak tensor corrections are usually buried under the dominating spin strength. In contrast, ℓ-forbidden transitions are

mainly governed by the tensor part, thus providing experimental insight into this otherwise hardly accessible contribution [16]. A detailed understanding of the tensor corrections is lacking and is the subject of current experimental and theoretical research (see e.g. [17]).

Application of the relativistic SU(2) symmetry leads to the specific predictions for the wave functions of pseudospin partners and for the strengths of M1 and GT transitions between them.

It has been tested for M1 transitions against experimental data with overall good agreement [9]. This motivates an analogous test for GT transitions, pursued in this thesis.

4.2. Dirac wave functions

The Dirac wave functions for the two states in the doublet are [18]

$$\Psi_{\tilde{n},\tilde{l},\tilde{j}=l+1/2,m} = (g_{\tilde{n}-1,\tilde{l},j}[Y_{\tilde{l}+1}\chi]_m^{j=\tilde{l}+1/2}, if_{\tilde{n},\tilde{l},j}[Y_{\tilde{l}}\chi]_m^{j=\tilde{l}+1/2})$$

$$\Psi_{\tilde{n},\tilde{l},\tilde{j}=l-1/2,m} = (g_{\tilde{n},\tilde{l},j}[Y_{\tilde{l}-1}\chi]_m^{(j=\tilde{l}-1/2)}, if_{\tilde{n},\tilde{l},j}[Y_{\tilde{l}}\chi]_m^{(j=\tilde{l}-1/2)}), \qquad (1)$$

where g, f are the radial wave functions, $Y_{\tilde{l}}$ are the spherical harmonics, χ is a two-component Pauli spinor, and $[\ldots]^{(j)}$ means coupled to angular momentum j. Note that the upper component of the $j=\tilde{l}-1/2$ wave function has the same radial quantum number as the lower component, whereas the upper component of the $j=\tilde{l}+1/2$ wave function has a radial quantum number one unit less than the lower component. The normalization of the wave function gives:

$$\int_0^\infty [g_{\tilde{n}',\tilde{l},j}^2 + f_{\tilde{n},\tilde{l},j}^2]r^2 dr = 1$$

$$j = \tilde{l} + 1/2, \tilde{n}' = \tilde{n} + 1; \ j = \tilde{l} - 1/2, \tilde{n}' = \tilde{n}$$

Pseudospin symmetry assumes that the spatial wave functions of the lower components of the doublet are equal and opposite in sign

$$f_{\tilde{n},\tilde{l},j=\tilde{l}+1/2,\rho}(r) = -f_{\tilde{n},\tilde{l},j=\tilde{l}-1/2,\rho}(r) = f_{\tilde{n},\tilde{l},\rho}(r). \qquad (2)$$

4.3. Magnetic dipole transitions between pseudospin partners

The relativistic magnetic dipole operator for a particle with charge e is given by [19]

$$\hat{\mu}_i = -\frac{e}{2}g_\rho(\vec{\alpha}\cdot\vec{r})_i + \mu_{A,\rho}\sigma_i \tag{3}$$

where $\vec{\alpha}$ is the usual Dirac matrix, $\vec{r}$ is the three space vector, $\rho=\pi$ for a proton and ν for a neutron, g_ρ is the orbital gyromagnetic ratio ($g_\pi = 1$, $g_\nu = 0$), and $\mu_{A,\rho}$ is the anomalous magnetic moment ($\mu_{A,\pi} = 1.793 \ \mu_0$, $\mu_{A,\nu} = -1.913 \ \mu_0$, where $\mu_0 = e\hbar/2Mc$ is the nuclear magneton). The magnetic moment is given in terms of the matrix element of this operator with $m = j$,

$$\mu_{j,\rho} = \left\langle \Psi_{\tilde{n},\tilde{l},j,m=j,\rho} \left| \hat{\mu} \right| \Psi_{\tilde{n},\tilde{l},j,m=j,\rho} \right\rangle \tag{4}$$

and the square root of the magnetic transition probability between two states in the doublet is given in terms of the reduced matrix element of this operator:

$$\sqrt{B(M1:\tilde{n},\tilde{l},j'\to\tilde{n},\tilde{l},j)_\rho} = \frac{1}{(2j'+1)}\left\langle \Psi_{\tilde{n}',\tilde{l},j',\rho} \left\| \hat{\mu} \right\| \Psi_{\tilde{n},\tilde{l},j,\rho} \right\rangle \tag{5}$$

4.4. Gamow-Teller transitions between pseudospin partners

The Gamow-Teller operator is given by

$$GT = \frac{g_A}{\sqrt{2}}\sigma\tau_\pm \ , \tag{6}$$

where g_A is the axial vector coupling constant ($g_A = 1.2670$) and $\tau_\pm$ are the isospin raising and lowering operators. Thus, the GT operator is of pure isovector nature. Using the Dirac wave function (1) the results

$$\sqrt{B(GT:\tilde{n},\tilde{l},j,\rho\to\tilde{n},\tilde{l},j,\bar{\rho})} = \sqrt{\frac{(j+1)}{j}}g_A\left(1-\frac{(2j+1)}{(j+1)}\int_0^\infty f_{\tilde{n},\tilde{l},j,\rho}f_{\tilde{n},\tilde{l},j,\bar{\rho}}r^2dr\right) \tag{7}$$

and

$$\sqrt{B(GT:\tilde{n},\tilde{l},j,\rho\to\tilde{n},\tilde{l},j,\bar{\rho})} = -\frac{g_A}{\sqrt{j(j+1)}}\left(j-(2j+1)\int_0^\infty f_{\tilde{n},\tilde{l},j,\rho}f_{\tilde{n},\tilde{l},j,\bar{\rho}}r^2dr\right) \tag{8}$$

are for the allowed transitions. For the ℓ-forbidden $j'=\tilde{l}+1/2\to j=\tilde{l}-1/2$ transition one finds

$$\sqrt{B(GT:\tilde{n},\tilde{l},j',\rho \to \tilde{n},\tilde{l},j,\overline{\rho})} = -\sqrt{\frac{2j+1}{2j'+1}}\sqrt{B(GT:\tilde{n},\tilde{l},j,\overline{\rho} \to \tilde{n},\tilde{l},j',\rho)}$$

$$= -\sqrt{\frac{2j+1}{j+1}}g_A\int_0^\infty f_{\tilde{n},\tilde{l},j',\rho}f_{\tilde{n},\tilde{l},j,\overline{\rho}}r^2 dr \tag{9}$$

where $\overline{\rho}=\pi$ if $\rho=\nu$ and $\overline{\rho}=\nu$ if $\rho=\pi$.

In the non-relativistic limit terms quadratic in f are ignored and one gets the usual results [18]:

$$\sqrt{B(GT:\tilde{n},\tilde{l},j,\rho \to \tilde{n},\tilde{l},j,\overline{\rho})} = \sqrt{\frac{(j+1)}{j}}g_A;\ j=\tilde{l}-1/2 \tag{10}$$

$$\sqrt{B(GT:\tilde{n},\tilde{l},j,\rho \to \tilde{n},\tilde{l},j,\overline{\rho})} = -\sqrt{\frac{j}{(j+1)}}g_A;\ j=\tilde{l}+1/2 \tag{11}$$

$$\sqrt{B(GT:\tilde{n},\tilde{l},j',\rho \to \tilde{n},\tilde{l},j,\overline{\rho})} = 0;\ j'\neq j \tag{12}$$

Thus, the strength of ℓ-forbidden GT transitions is predicted to be zero.

Using pseudospin symmetry (2), there is only one unknown for the GT transitions and hence each transition is related to the other [18]. Assuming the case $j'=\tilde{l}+1/2 \to j=\tilde{l}-1/2$, the ℓ-forbidden GT matrix element is related to the allowed $j\to j$ and $j'\to j'$ transitions by:

$$\sqrt{B(GT:\tilde{n},\tilde{l},j',\rho \to \tilde{n},\tilde{l},j,\overline{\rho})} = -\sqrt{\frac{j}{(2j+1)}}\left(\sqrt{B(GT:\tilde{n},\tilde{l},j,\rho \to \tilde{n},\tilde{l},j,\overline{\rho})} - \sqrt{\frac{j+1}{j}}g_A\right) \tag{13}$$

$$\sqrt{B(GT:\tilde{n},\tilde{l},j',\rho \to \tilde{n},\tilde{l},j,\overline{\rho})} = \sqrt{\frac{(j+2)(2j+1)}{2j+3}}\left(\sqrt{B(GT:\tilde{n},\tilde{l},j',\rho \to \tilde{n},\tilde{l},j',\overline{\rho})} + \sqrt{\frac{j+1}{j+2}}g_A\right) \tag{14}$$

For the allowed transitions the relation

$$\sqrt{B(GT:\tilde{n},\tilde{l},j',\rho \to \tilde{n},\tilde{l},j,\overline{\rho})} = \sqrt{B(GT:\tilde{n},\tilde{l},j',\overline{\rho} \to \tilde{n},\tilde{l},j,\rho)} \tag{15}$$

holds. It also follows from isospin symmetry, but if pseudospin symmetry is conserved than the relation holds even though isospin may be violated; i.e. $f_{\tilde{n},\tilde{l},\pi}\neq f_{\tilde{n},\tilde{l},\nu}$.

4.5. Application of pseudospin symmetry to experimental data

The $B(GT)_{exp}$ values can be calculated from experimental β-decay data with the appropriate spin and isospin quenching values for the initial and final states. The experimental results are usually expressed by a so-called ft-values representing the product of the half-life time and phase space factor. The relation between the values ft and $B(GT)_{exp}$ has the following form

$$B(GT)_{exp} = \frac{6146}{ft} - B(F),$$ (16)

where the factor 6146 is taken from [20]. The quantity B(F) denotes the Fermi transition strength. This strength contributes to transitions between mirror nuclei only. In the present case only examples with $T = 1/2$, $T_z^i = 1/2$, $T_z^f = -1/2$ are calculated. Thus it has the value $B(F) = T(T+1) - T_z^i \cdot T_z^f = 1$. Contributions of isospin mixing and radiative corrections to B(F) are typically < 1% and are neglected here. The experimental ft values are taken from [21].

With the formulas (13) and (14) one is now able to make pseudospin symmetry predictions for the ℓ-forbidden GT transitions. As the equations (13,14) hold for the pure single particle transitions, the corresponding single particle B(GT) values must be extracted from the data. The relation between single particle and experimental values can be expressed as (see e.g. [22]):

$$B(GT)_{s.p.} = \frac{2j_f + 1}{n_i^p \cdot n_f^h} \cdot B(GT)_{exp}$$ (17)

Here j_f is the total angular momentum of the final state, n_i^p gives the number of particles in initial orbit and n_f^h the number of holes in final orbit. It is assumed here that all shell model orbits are filled up successively, as in the independent particle model.

Since all experimental data are from ground state β-decay for allowed $j \rightarrow j$ transitions the corresponding forbidden transitions are always of type $j \rightarrow j'$, while formulas (13, 14) are given for $j' \rightarrow j$. This must be corrected by introducing a statistical factor (see e.g. (9))

$$B(GT : j \to j') = \frac{(2j'+1)}{(2j+1)} B(GT : j' \to j). \tag{18}$$

Experimentally one obtains B(GT), but in equations (13, 14) the expression $\sqrt{B(GT)}$ shows up. The sign of square root is unknown, therefore the sign that leads to a better agreement with the experimental data is selected. In light nuclei, where shell model calculations of the full major shell are possible, the assumed signs agree with the calculated ones [23].

Generally the calculations of B(GT) for the forbidden transitions were performed for two values of g_A. The first one assumes $g_A = 1.267$ of the free nucleon case. The second one takes into account the phenomenon of spin quenching in nuclei [15]. Although a weak mass dependence of the quenching is reported [24], for simplicity a constant factor of 0.7 (i.e. $g_{A,eff} = 1.267 \cdot 0.7 = 0.887$) is assumed.

Alternatively, one can extract a quenching factor $g_{A,eff}$ necessary to obtain a quantitative agreement with pseudospin symmetry. All the relevant data for the calculations and their results are presented in table 2.

Table 2: Experimental data and results. The quantities are: $\tilde{l}$ - pseudo-orbital momentum of the pseudospin partners; A_i, A_f - initial and final isotops respectively, $s.p.o._i$, $s.p.o._f$ - single particle orbits in initial and final nuclei; E_x - energy levels of daughter nucleus; $B(GT)_{exp}$ - experimentally measured value of transition strength; $B(GT)_{theor}$ - calculated value for $g_A = 1.267$; $B(GT)'_{theor}$ - calculated value for $g_A = 0.887$; $g_{A,eff}$ - values calculated with the assumption that pseudospin symmetry is valid.

$\tilde{l}$	A_i	$s.p.o._i$	A_f	$s.p.o._f$	$E_x(MeV)$	$B(GT)_{exp}$	$B(GT)_{theor}$	$B(GT)'_{theor}$	$g_{A,eff}$
1	$^{35}_{18}Ar_{17}$	$1d_{3/2}$	$^{35}_{17}Cl_{18}$	$1d_{3/2}$	g.s.	$6,56\cdot10^{-2}$			
				$2s_{1/2}$	1.219	$4.88\cdot10^{-2}$	0.187	$7.14\cdot10^{-2}$	0.840
1	$^{35}_{19}K_{16}$	$1d_{3/2}$	$^{35}_{18}Ar_{17}$	$1d_{3/2}$	g.s.	$6.01\cdot10^{-2}$			
				$2s_{1/2}$	1.184	$9.74\cdot10^{-3}$	0.221	$9.3\cdot10^{-2}$	0.544
1	$^{39}_{20}Ca_{19}$	$1d_{3/2}$	$^{39}_{19}K_{20}$	$1d_{3/2}$	g.s.	$4.08\cdot10^{-1}$			
				$2s_{1/2}$	2.522	$5.35\cdot10^{-4}$	$3.65\cdot10^{-2}$	$7.27\cdot10^{-4}$	0.878
2	$^{49}_{20}Ca_{29}$	$2p_{3/2}$	$^{39}_{21}Sc_{28}$	$2p_{3/2}$	3.082	$5.18\cdot10^{-2}$			
				$1f_{5/2}$	4.072	$4.66\cdot10^{-2}$	1.113	0.386	0.400

$\tilde{l}$	A_i	s.p.o.$_i$	A_f	s.p.o.$_f$	$E_x(MeV)$	$B(GT)_{\text{exp}}$	$B(GT)_{theor}$	$B(GT)'_{theor}$	$g_{A,\text{eff}}$
2	$^{57}_{28}Ni_{29}$	$2p_{3/2}$	$^{57}_{27}Co_{30}$	$2p_{3/2}$	1.379	$1.41\cdot10^{-2}$			
				$1f_{5/2}$	2.135	$4.56\cdot10^{-5}$	1.261	0.571	0.099
2	$^{57}_{29}Cu_{28}$	$2p_{3/2}$	$^{57}_{28}Ni_{29}$	$2p_{3/2}$	g.s.	$3.14\cdot10^{-1}$			
				$1f_{5/2}$	0.769	$2.23\cdot10^{-2}$	0.65	0.192	0.588
2	$^{59}_{29}Cu_{30}$	$2p_{3/2}$	$^{59}_{28}Ni_{31}$	$2p_{3/2}$	g.s.	$5.72\cdot10^{-2}$			
				$1f_{5/2}$	0.339	$9.01\cdot10^{-3}$	0.946	0.366	0.283
2	$^{59}_{30}Zn_{29}$	$2p_{3/2}$	$^{59}_{29}Cu_{30}$	$2p_{3/2}$	g.s.	$4.41\cdot10^{-1}$			
				$1f_{5/2}$	0.914	$2.56\cdot10^{-2}$	0.672	0.204	0.680
2	$^{61}_{29}Cu_{32}$	$2p_{3/2}$	$^{61}_{28}Ni_{33}$	$2p_{3/2}$	g.s.	$5.23\cdot10^{-2}$			
				$1f_{5/2}$	0.067	$3.01\cdot10^{-3}$	1.111	0.471	0.234
2	$^{61}_{30}Zn_{31}$	$2p_{3/2}$	$^{61}_{29}Cu_{32}$	$2p_{3/2}$	g.s.	$2.42\cdot10^{-2}$			
				$1f_{5/2}$	0.970	$5.11\cdot10^{-4}$	1.126	0.481	0.144
2	$^{61}_{31}Ga_{30}$	$2p_{3/2}$	$^{61}_{30}Zn_{31}$	$2p_{3/2}$	g.s.	$4.4\cdot10^{-1}$			
				$1f_{5/2}$		$4.66\cdot10^{-2}$	0.672	0.204	0.737
2	$^{65}_{28}Ni_{37}$	$1f_{5/2}$	$^{65}_{29}Cu_{36}$	$1f_{5/2}$	1.115	$1.1\cdot10^{-2}$			
				$2p_{3/2}$	1.623 g.s.	$1.63\cdot10^{-3}$	0.433	0.194	0.447
2	$^{65}_{30}Zn_{35}$	$1f_{5/2}$	$^{65}_{29}Cu_{36}$	$1f_{5/2}$	1.115	$7.94\cdot10^{-3}$			
				$2p_{3/2}$	g.s.	$2.18\cdot10^{-4}$	0.48	0.226	0.084
2	$^{67}_{31}Ga_{36}$	$2p_{3/2}$	$^{67}_{30}Zn_{37}$	$2p_{3/2}$	0.393	$3.53\cdot10^{-2}$			
				$1f_{5/2}$	0.858	$1.41\cdot10^{-2}$	1.178	0.515	0.269
2	$^{69}_{29}Cu_{40}$	$2p_{3/2}$	$^{69}_{30}Zn_{39}$	$2p_{3/2}$	0.834	$2.82\cdot10^{-2}$			
				$1f_{5/2}$	0.531	$3.46\cdot10^{-3}$	0.808	0.629	0.191
3	$^{111}_{51}Sb_{60}$	$2d_{5/2}$	$^{111}_{50}Sn_{61}$	$2d_{5/2}$	1.155	$2.39\cdot10^{-2}$			
				$1g_{7/2}$	g.s.	$4.88\cdot10^{-3}$	1.003	0.445	0.210
3	$^{115}_{51}Sb_{64}$	$2d_{5/2}$	$^{115}_{50}Sn_{65}$	$2d_{5/2}$	0.987	$3.54\cdot10^{-3}$			
				$1g_{7/2}$	0.614	$2.45\cdot10^{-4}$	1.152	0.547	0.068
3	$^{117}_{51}Sb_{66}$	$2d_{5/2}$	$^{117}_{50}Sn_{67}$	$2d_{5/2}$	1.019 1.180	$2.58\cdot10^{-3}$			
				$1g_{7/2}$	0.711	$1.73\cdot10^{-4}$	1.164	0.554	0.058
3	$^{119}_{53}J_{66}$	$2d_{5/2}$	$^{119}_{52}Te_{66}$	$2d_{5/2}$	0.321	$7.74\cdot10^{-4}$			
				$1g_{7/2}$	0.360	$1.54\cdot10^{-3}$	1.12	0.579	0.068
3	$^{123}_{53}J_{70}$	$2d_{5/2}$	$^{123}_{52}Te_{69}$	$2d_{5/2}$	0.505	$3.46\cdot10^{-4}$			
				$1g_{7/2}$	0.490	$1.94\cdot10^{-6}$	1.216	0.589	0.018

4.6. Discussion of the results

In fig. 8 the experimental and theoretically predicted values of B(GT) of ℓ-forbidden transitions and the g_A value for the free nucleon case are shown. Ideal

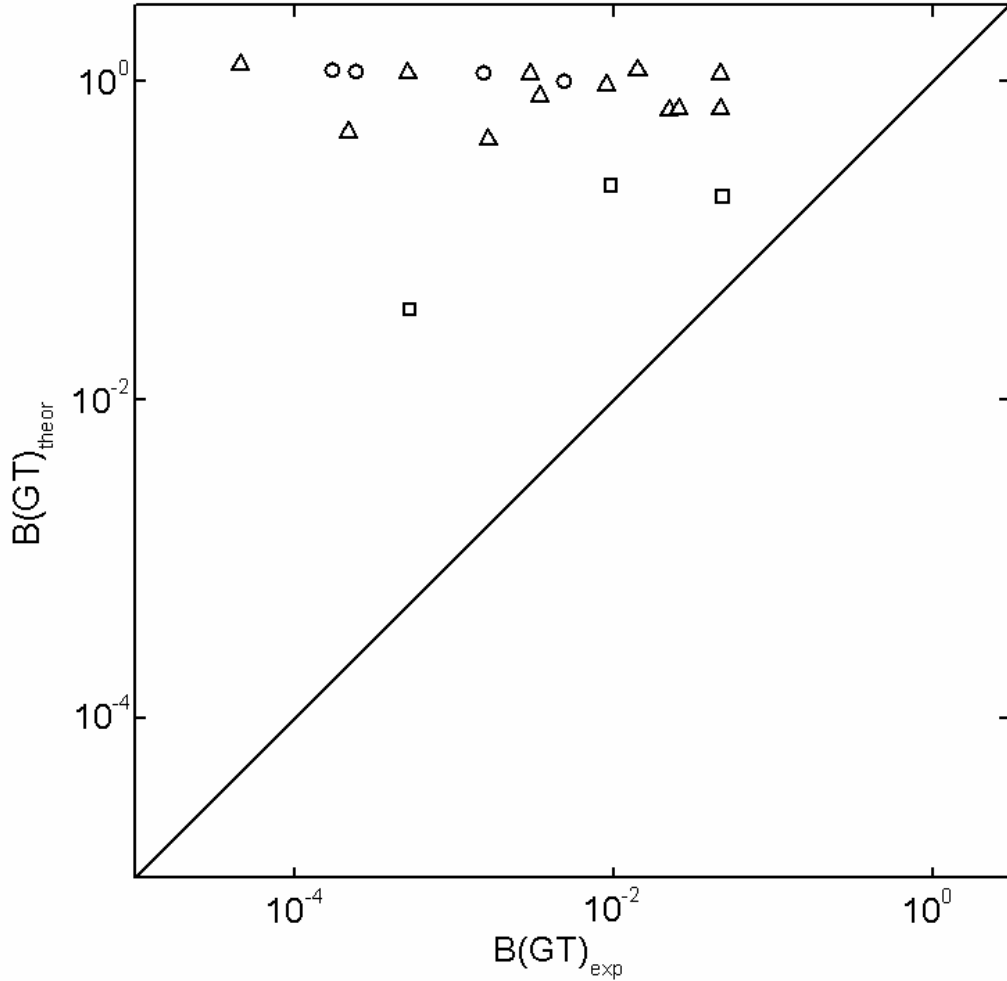correspondence would be achieved for the points lying on the straight line given by $B(GT)_{theor} = B(GT)_{exp}$.

Fig. 8: Comparison of experimental B(GT) values of ℓ-forbidden transitions with the predictions assuming pseudospin symmetry and $g_A = 1.267$. The symbols represent cases with different pseudo-orbital angular momentum. (□: $\tilde{l} = 1$; Δ: $\tilde{l} = 2$; ○: $\tilde{l} = 3$)

The agreement is poor for all cases. The pseudospin symmetry predictions of $B(GT)_{theor}$ are large and comparable to the values for allowed transitions.

The effect of taking into account the spin quenching of g_A is demonstrated in fig. 9. In this case the agreement is generally improved. Still, the correspondence is rather poor for the majority of cases. Good agreement is found for two transitions with $\tilde{l} = 1$. Also, some transitions with $\tilde{l} = 2$ are not too far from the straight line.
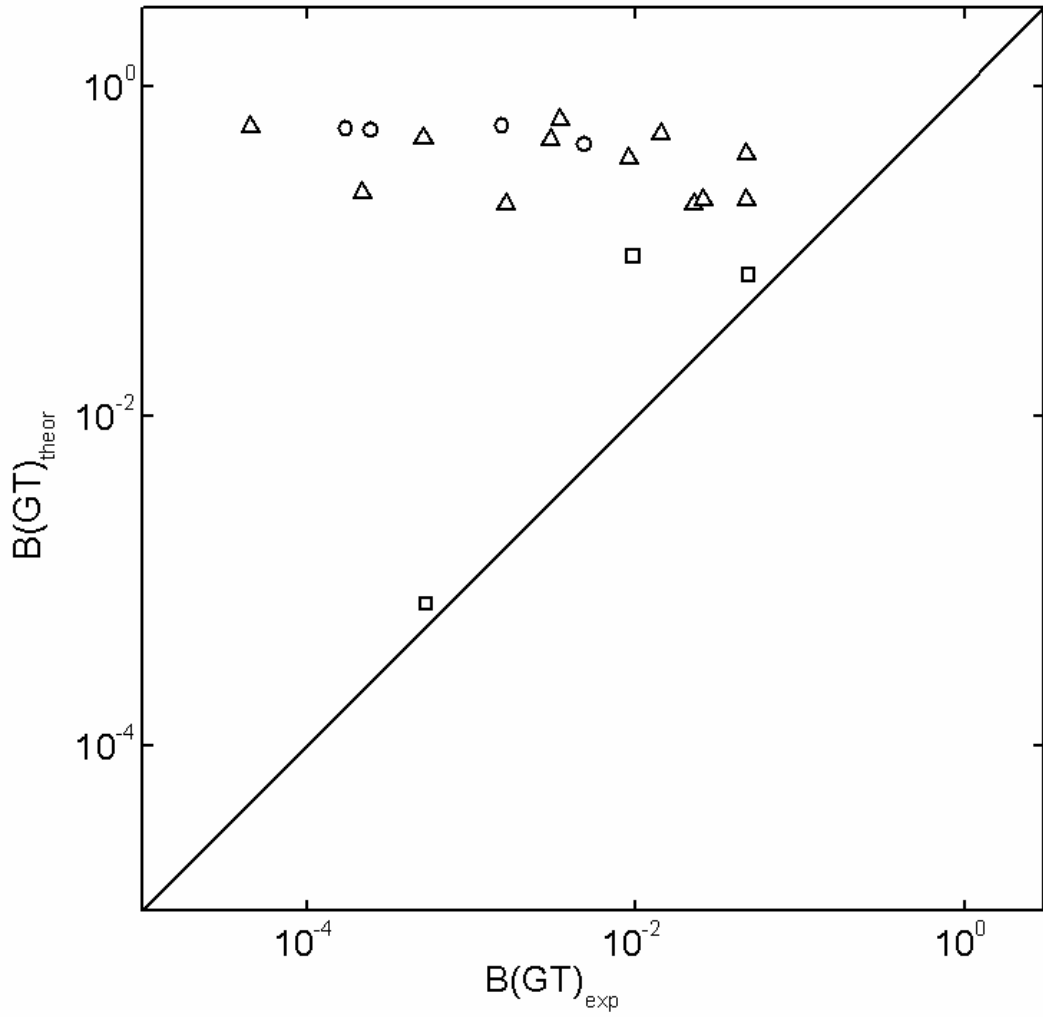
Fig. 9: Same as fig. 8, but assuming $g_A = 0.887$. ($\square$: $\tilde{l} = 1$; Δ: $\tilde{l} = 2$; $\circ$: $\tilde{l} = 3$)

Finally fig. 10. represents the values of g_A, needed to fulfill the agreement between experiment and pseudospin symmetry predictions.
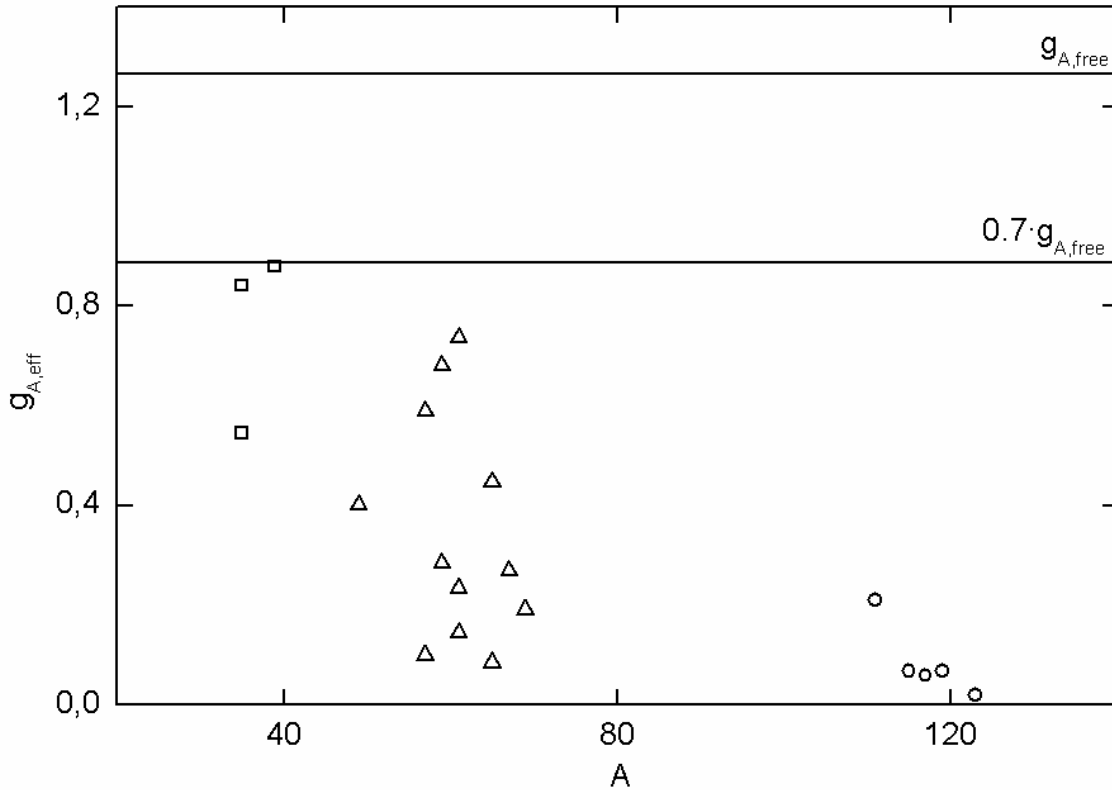
Fig. 10: Effective values of g_A, necessary to obtain the agreement of the experimental data with pseudospin symmetry predictions (eqs. (13, 14)). ($\square$: $\tilde{l} = 1$; $\triangle$: $\tilde{l} = 2$; $\circ$: $\tilde{l} = 3$)

While generally the results of fig. 9 are also reflected here, it becomes clear that the quality of pseudospin symmetry predictions differs essentially with $\tilde{l}$. For $\tilde{l} = 1$ (Z, N=20 shell closure) the correspondence is reasonable. For $\tilde{l} = 2$ (Z, N = 28) it is mediocre. For the majority of the points unrealistically large quenching factors would be needed. For $\tilde{l} = 3$ (N = 82) the agreement is generally very poor.

4.7. Conclusion

Predictions of relativistic pseudospin symmetry for ℓ-forbidden GT transitions were tested using available experimental data from ground state β-decay. Generally, the agreement is much poorer than that for the similar analysis of ℓ-forbidden M1 transitions [9]. The results improve if quenching of the axial vector current is taken into account, but they are still far from satisfactory.

30

Strong dependence of the agreement of theory and experiment on $\tilde{l}$ was found:

- reasonable agreement for 2s-1d shell,

- mediocre agreement for 2p-1f shell,

- poor for agreement 3s-2d-1g shell.

The present approach is limited, however, because of the independent particle model. In reality the residual interaction leads to the redistribution of particles over the valence orbits (softering of the Fermi surface). Thus, the comparison could be improved in the future by using e.g. BCS calculations to determine the occupation numbers n_i^p and n_f^h in (16).

Appendixes

A. LabView code for the program parts

A.1. Original SubVI's

The program itself is organized as virtual instrument (VI). During the execution it has to perform some repeating parts. In order to make the program code easy readable and to speed up the program creation some original independent subprograms (SubVI's) were elaborated.

A.1.1. Form IXE command SubVI

All sending commands should have a look <STX><Command><ETX> <CR><LF>. A special SubVI is used for this purpose. On the only input comes a simple text command (for example: XMA), and from the output comes also this command but in IXE acceptable appearance.

A.1.2. Dynamic timing SubVI

Another special SubVI is used to stop the program execution for some time necessary for the answer from IXE to appear in the ports buffer. This time depends on command string length and port parameters. The SubVI has the only input, on which the command string comes. It takes the length of this string and calculates the pause duration, depending on the port parameters. Two optional outputs show command string length and duration time.

A.1.3. Send command SubVI

The whole performance of the system is grounded on sending standard commands to IXE and receiving the answer on them from it. Both sending and receiving performs original "Send command SubVI".

1. At the first step command, incoming from the IXE command input, is influenced to fit LabView requirements [25]. It is made by "Form IXE command SubVI".

2. Then, the program sends the command to the destination device, selected by VISA resource name.

3. After sending a command one should wait for some time, depending on the command length, when the answer of the device appears in the ports buffer. The duration time is calculated by "Dynamic timing SubVI".

4. After the answer appears in the buffer, the program defines the number of bytes in port & then reads the exact number of bytes in order to exhaust the buffer.

5. The read answer goes in hexadecimal form to the output.

6. Also the program looks through the answer for ACK symbol (Hex: 06, Dec: 6). If ACK symbol is presented in the answer, "Nak" output receives value "False", if not – then "True". This is made with the purpose of easy error control. ACK symbol tells user that command is accepted by IXE. If there is no ACK symbol in the answer, the command was not accepted, nothing was done & there was no any data in the port. Attaching a Boolean indicator to "Nak" output user is always able to see if an error occurs.

7. All possible errors, that can be recognized and handled by LabView, are also controlled in each step of the execution of the program. If any appears, it can be pointed out by standard "LabView simple error handler" connected to the error output.

A.1.4. Read input status SubVI

One of the most common tasks performed by the program is reading the current state of one of the seven used inputs. All necessary for that actions are gathered into the original "Read input status SubVI". The LabView scheme of this SubVI is shown in fig. 11. This SubVI has two own inputs and four own outputs. Their purpose is described below.

1. Visa resource name input. It should be wired as standard LabView VISA resource name.

2. IXE input number. It should be wired as two position text, pointing status of which input to read. For example: 02.

3. Input status text output. It returns text 1 or 0. 1 reports that input status is "On", 0 – that it is "Off".

4. Input status Boolean output. It returns Boolean 1 or 0. Interpretation is the same to №3.

5. Acknowledgement status output. It returns Boolean signal. "False" reports acknowledgement (ACK), "True" – negative acknowledgement (NAK).

6. Error output. It returns standard LabView error signal.

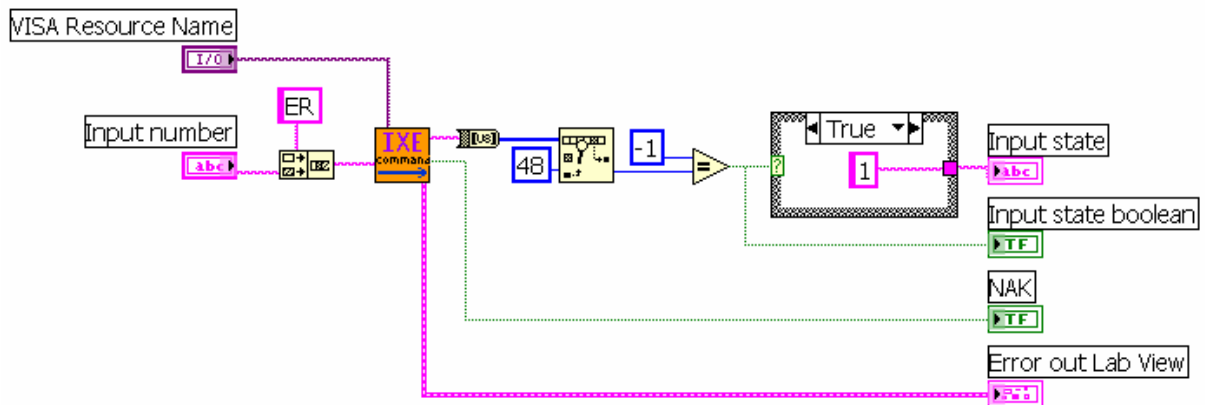Fig. 11: Scheme of the "Read input status SubVI".

A.1.5. Change output status SubVI

As it was written in 2.3. the program uses four outputs to control flip-target, laser and chamber light. The same operations take place to change any of the output's status, so it is convenient to create a SubVI which will be responsible for that.

In the activation part of the program all the outputs receive their default values, that are "0". When the program reaches the work part, user becomes able to change the status of any output. LabView scheme of this SubVI is shown in fig. 12.

First the SubVI reads the number of output and its current state. Then it sends the command to IXE to set the state of this output to the opposite value.

If the command was successfully processed then the appropriate front panel indicators (Pos. 13, 15, 17, 19 in fig. 7) show the new output state. If not, then the output's state does not change and the error indicator (Pos. 6) lights up.
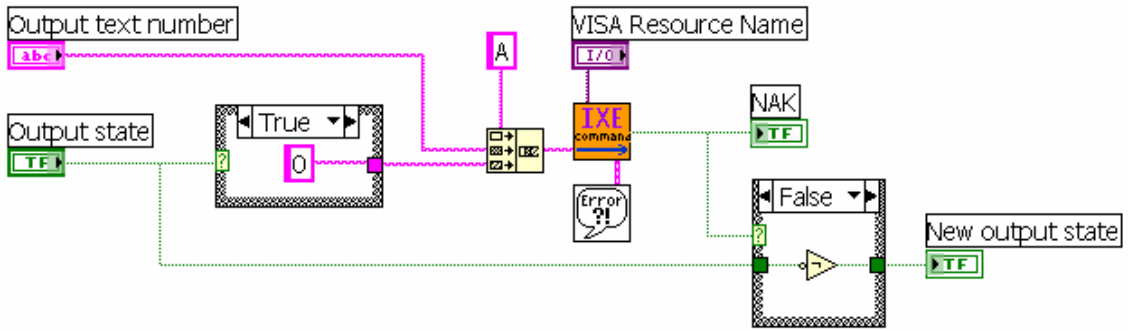
Fig. 12: Scheme of the "Change output status SubVI".

A.2. Initialization

The LabView scheme of the initialization frame is shown in fig. 13.
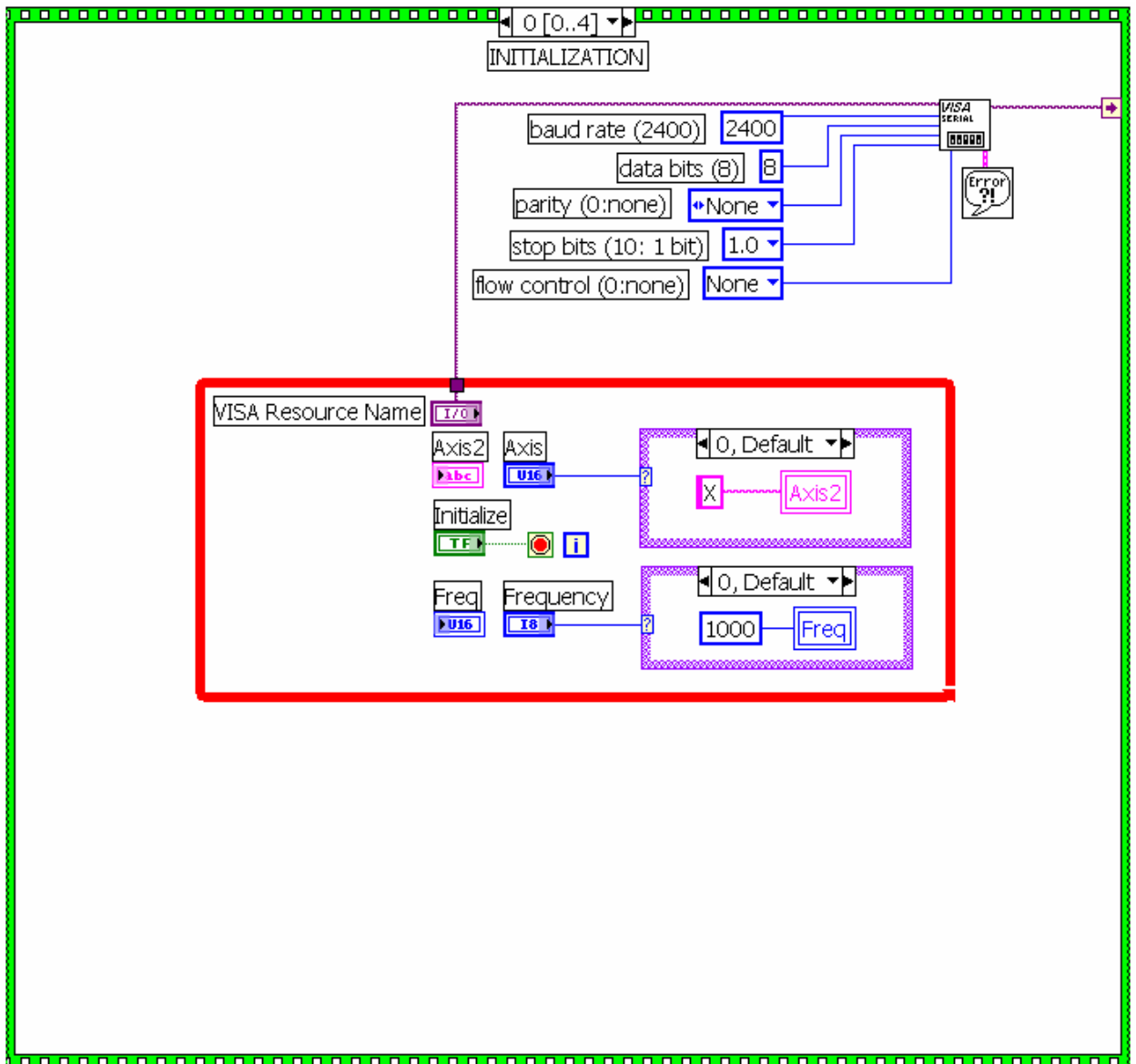

Fig. 13: Initialization frame.

First of all IXE requires some parameters which are necessary for further operation such as name and settings of the computer port, the working frequency and axis. The initialization frame implements these tasks.

This frame is executed after the start of the program. The user has to set the name of the computer port (Pos. 1 in fig. 7), the name of axis (Pos. 2) and the working frequency (Pos. 3) on the front panel.

After the "Initialize IXE" button is pressed, the chosen values are stored into the corresponding variables and the program tries to establish a connection between PC and IXE through the given port. If it succeeds, the initialization frame is finished and the activation frame begins. If not, the error indicator (Pos. 6 in fig. 7) lights up or an error message appears (it depends on the operating system on PC).

A.2.1. Determination of the port parameters

In order to find out the necessary port parameters with which IXE works correctly a simple symbol "a" (DEC code: 97) has been sent to the port. It is not a valid IXE command, so according to the documentation [25] the answer should look like:

<STX><NAK><ETX><CR><LF>

The meaning of these abbreviations can be found in every ASCII table (Appendix B). IXE returned following (50 bits):

0010000001010000010101100000010101100001001010000

As 5 bytes were expected, then this string is divided into five equal parts. Locating them one under another, one obtains the following:

0010000001
0101010001
0110000001
0101100001
0010100001

36

From here it becomes clear that each byte has 8 data bits, starting from 0 (start bit) and ending with 1 (one stop bit). It is also obvious that the flow has no parity control. Finally, the obtained answer can be interpreted next way:

Start bit	*1	*2	*4	*8	*16	*32	*64	*128	Stop bit	parity	DEC	ASCII	description
0	0	1	0	0	0	0	0	0	1	1	2	STX	Start of text
0	1	0	1	0	1	0	0	0	1	1	21	NAK	Negative acknowledge
0	1	1	0	0	0	0	0	0	1	0	3	ETX	End of text
0	1	0	1	1	0	0	0	0	1	1	13	CR	Carriage return
0	0	1	0	1	0	0	0	0	1	0	10	LF	Line feed (new line)

In such interpretation the answer coincides with the predicted one. Thus IXE works with the following port parameters:

Baud rate: 2400 (standard)

Data bits: 8

Parity: none

Stop bits: 1

Flow control: none

A.3. Activation

The activation frame consists of four own successive parts which are organized into four subframes. The LabView scheme of the activation frame is shown in fig. 14.

Before any action with the stepper motor, it should be activated. This is achieved by sending the motor activation command (XMA) to IXE in the first subframe.

Then the frequency on which the motor will operate must be set. It can be done by writing a necessary value to the IXE parameter 04 with the help of the command XP04Sxxxx, where xxxx is replaced by the desirable number, representing a frequency in steps per second. The second subframe is responsible for that.
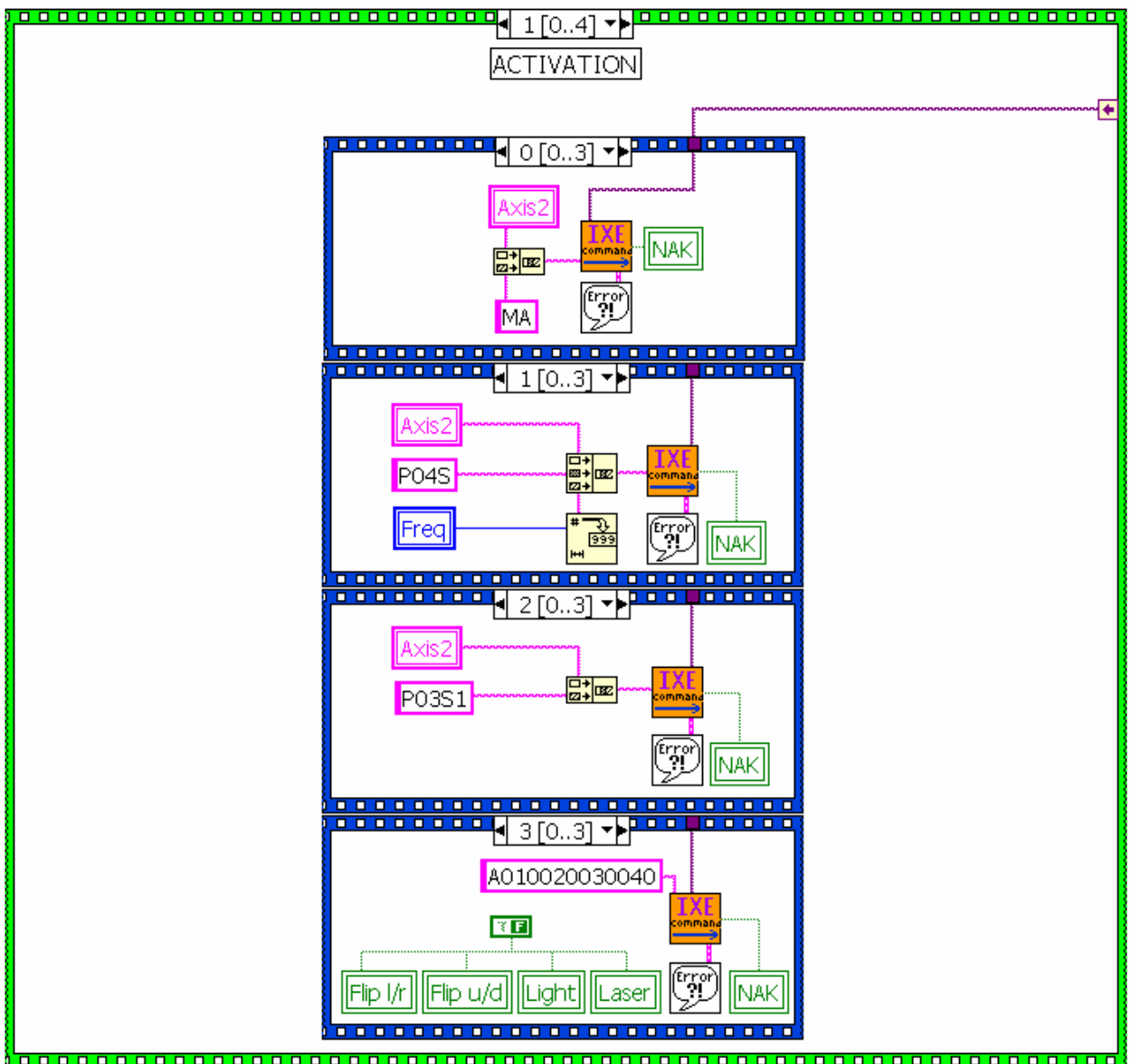
Fig. 14: Activation frame.

The frequency value comes from the pull down menu (Pos. 3 in fig. 7). There are three possible values that can be accepted as a frequency: 1000, 500 or 200 steps per second. The reason for choosing exactly these values is explained further in A.5.3.

In the third subframe the conversion factor is selected. The conversion factor is used when LabView does not operates with the steps. In this program, however, exactly steps are used, so this factor must be set to 1. IXE parameter 03 is responsible for that and sending of a command XP03S1 provides the necessary setting.

At the start of the program one is not able to determine the states of the outputs, so the only way to control them is to set them manually. In this program all the states of the outputs at the beginning are set to "0" in the fourth subframe. During the operation the user can always change the status of each of the four outputs.

A.4. Calibration

When the program starts, it is not known in which position the main target is situated. In order to determine it, the target is moved to the bottom position.

This is implemented with the cycle in which the command to move 0.5 centimeter down or to stop if the bottom position attained is sent. One has to wait for some time while the motor is moving, because IXE is not able to accept commands during that time. After the motor stops, the input 02 status request is sent. If the target is in its bottom position then input status is 0, current position indicator is set to 0.0000 and the calibration ends. If it is not then the cycle goes to its next iteration.

The LabView scheme of the calibration frame is shown in fig. 15. The algorithm is implemented as a three subframe structure. In the first frame the moving command is sent, in the second one the delay time is calculated and in the third one the program asks if the bottom position is reached.

After the calibration is finished the program is ready to work with the main and flip-targets. In the beginning the main target is in the bottom position, the flip-target is down, light and laser are off.
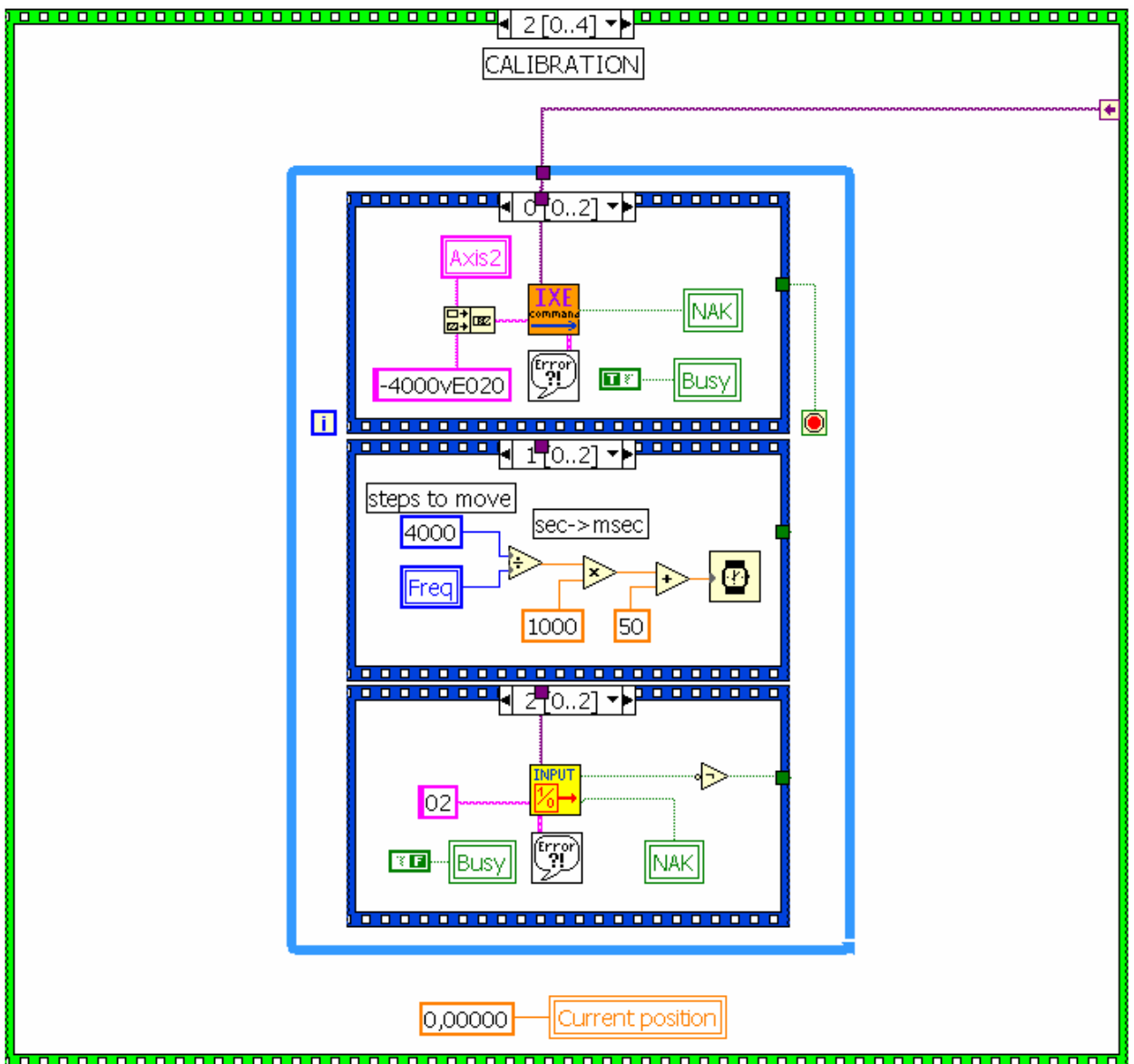
Fig. 15: Calibration frame.

A.5. Work

The work frame is organized as a cycle which repeats unless the end button is pressed. Inside this cycle the work can be divided into two big parts. The first one is performed when the button "Go" has been pressed (named moving case), the second one – if not (interface case). First the interface case will be depicted and then – the moving case.

A.5.1. Work – interface case

If the "Go" button was not pressed, an interface case is realized inside the work cycle. It starts from the successive requests for the state of flip u/d (Pos. 12 in

40

fig. 7), flip l/r (Pos. 14), light (Pos. 16) and laser (Pos. 18) buttons. If any has been pushed from the last work cycle iteration, then the program performs all the necessary actions for switching the corresponding device into the opposite position.
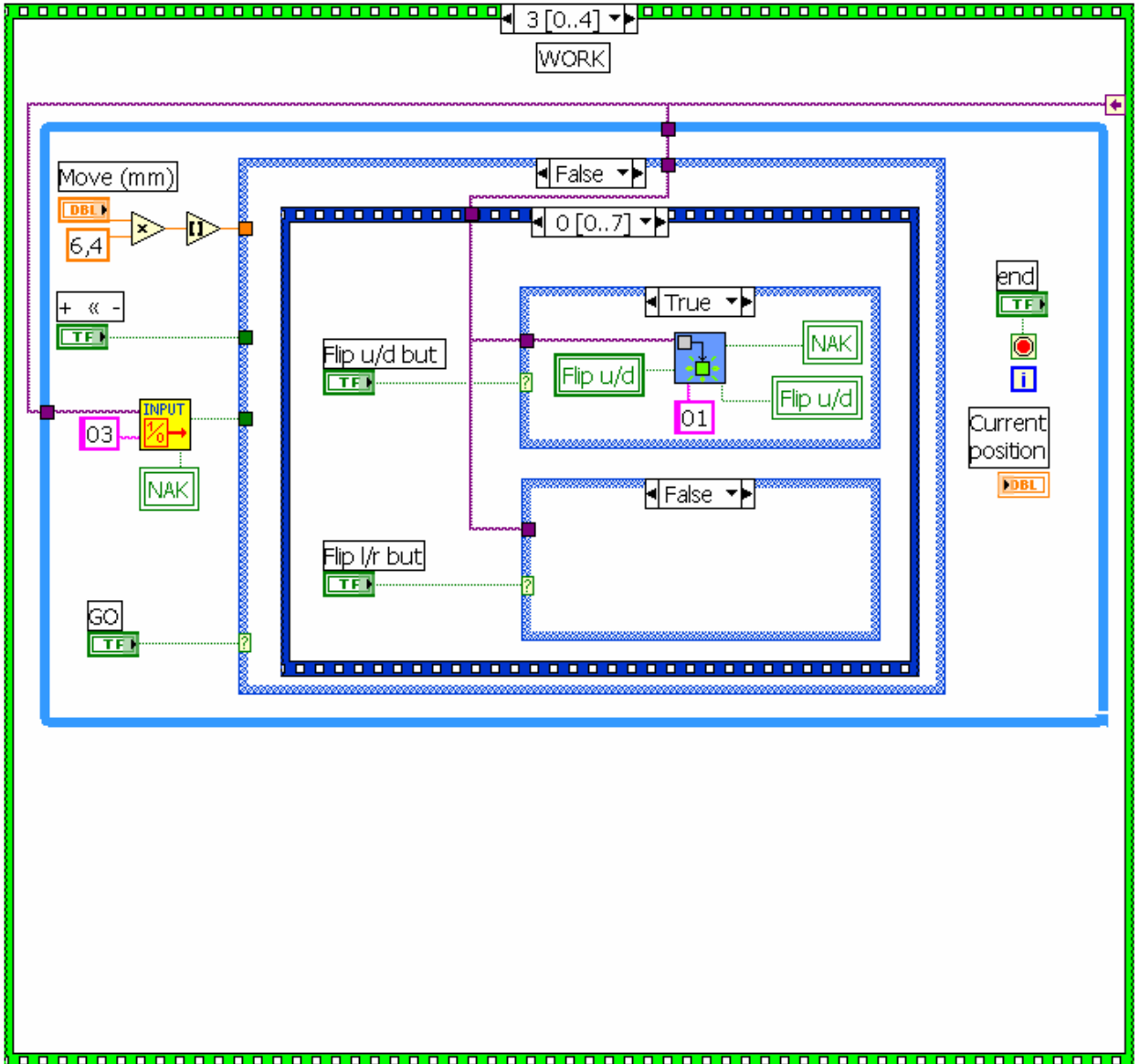
Fig. 16: Work frame, interface case LabView scheme №1

In fig. 16 the implemented LabView scheme is shown when the flip u/d button has been pushed. So, with the help of "Change output status SubVI" the program flips the flip-target up or down. In the next frame of this structure the same is performed with the light and laser buttons.

Then after processing these four outputs the program begins the successive questioning of the six input states (excluding input 03). In fig. 17 one can see the

request for the input 01 state which is responsible for top position of the main target indication.
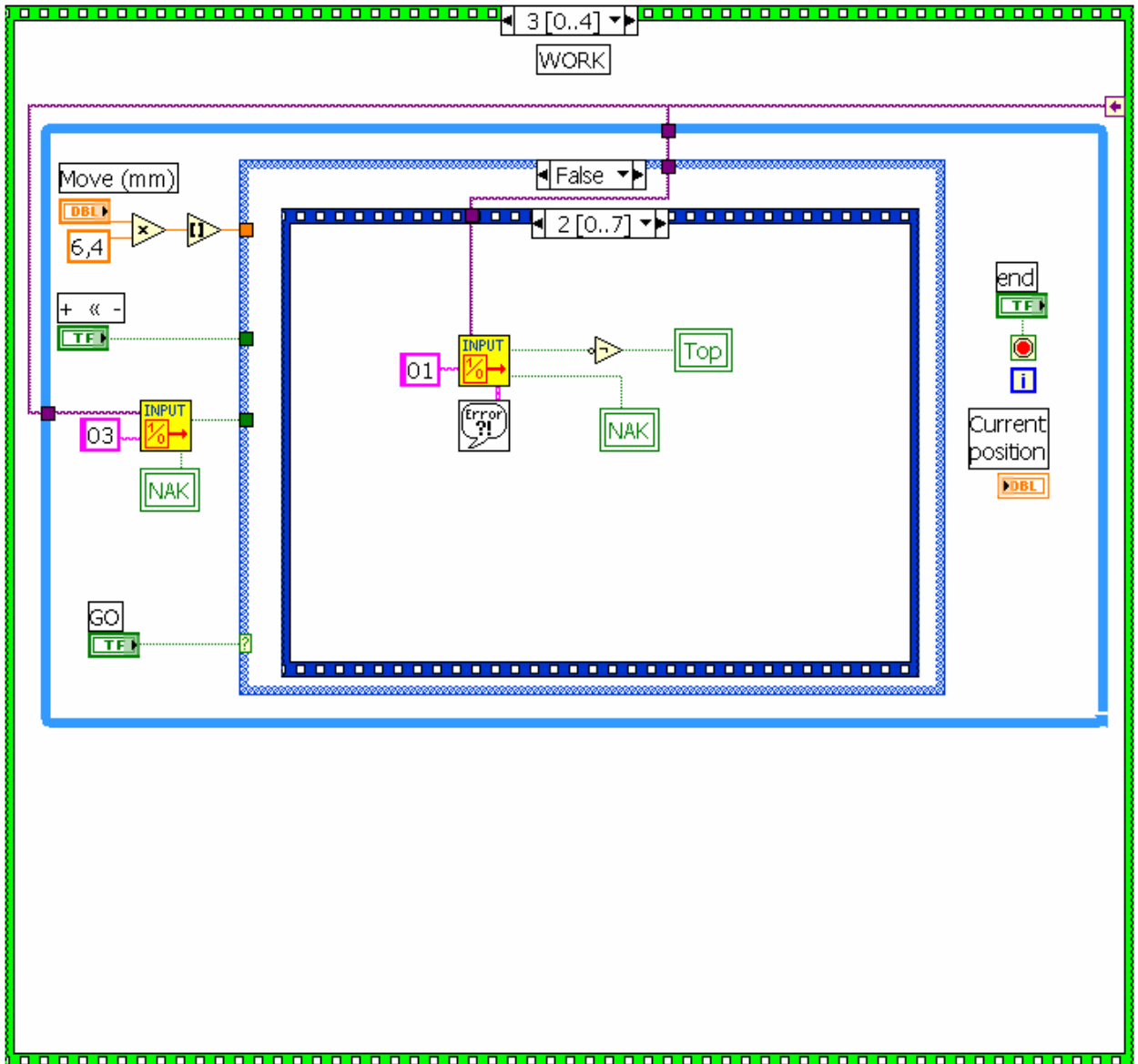
Fig. 17: Work frame, interface case LabView scheme №2

The result of this questioning is represented on the front panel top and bottom position indicators and also in the inputs state indicators (Pos. 5 in fig. 7).

A.5.2. Work – moving case

Another action takes place when the "Go" button has been pressed. The following program deeds are based on the next principle. When the motor is moving the eight magnets situated on the rotating ring pass successively the

42

detecting trigger that is connected to input 03. So the status of the input 03 changes every 1/16 revolution.

This makes it possible to realize the following algorithm for controlling the current position of the main target.

1. First the program reads the current state of input 03.

2. Then it converts the value entered in the corresponding field (Pos. 21 in fig. 7) into the amount of 1/16 revolution, necessary to move the target on the given distance.

3. The command to move 1/8 revolution or to stop if the input 03 changes its state is sent. At normal operation the state of input 03 always changes before the motor has been moved on 1/8 revolution.

4. At the end of the motion the program reads again the state of input 03. If it has changed the motor had moved into 1/16 revolution that is equal to 0.15625 mm in linear scale. If it has not changed then the magnetic coupling is missing and the program generates an error message. More about magnetic coupling is written in A.5.4. Here one should also show the compliance between linear, rotating and internal motor scales:

$$1 \text{ revolution} = 2.5 \text{ mm} = 2000 \text{ steps}$$
$$1 \text{ mm} = 0.4 \text{ revolution} = 800 \text{ steps}$$

7. If everything is correct the current position indicator (Pos. 7-8 in fig. 7) adds or subtracts the number of 0.15625 to the current value.

8. If the top or bottom position is reached the cycle stops immediately, if not – it continues with the steps 3-5 of this list the remained number of times, defined in the step 2.

9. With the last iteration the moving case is finished.

A.5.3. Definition of the working frequencies

The algorithm of controlling the target position, described in A.5.2. does not work in the all possible frequencies, it has an upper boundary. The experiment shows that the maximal allowed frequency is 1000 steps per second.

This experiment consisted of the cycle in which the command to move 250 steps (1/8 revolution) or until the input 03 state changes has been sent to IXE. The cycle had 16 iterations. The result obtained is shown in table 3.

Table 3: Results of the experiment on definition the upper boundary of the frequency, with which the algorithm of controlling the target position is valid.

Frequency	Total steps to move	Steps made	Steps per iteration
2000	4000	4000	250 (1/8 revolution)
1500	4000	4000	250 (1/8 revolution)
1000	4000	2000	125 (1/16 revolution)
500	4000	2000	125 (1/16 revolution)

From these results it becomes clear, that for the frequencies above 1000 the motor moves 1/8 revolution faster than IXE can recognize the change of the input 03 state. Because of that in the present program the frequency values of 1000, 500 and 200 steps per second are used.

A.5.4. Magnetic coupling between motor parts

The stepper motor itself consists of two parts separated with the aluminum partition. The motion is transferred from one part to another through the magnetic coupling. It means that each part of the motor has sixteen magnets in two circles one right opposite another. And when one part is moving, another repeats the motion due to the magnetic strengths.

The reason of such a construction is that a motor needs an oiling, that negatively affects the vacuum in the vacuum chamber. So the motor is divided into two parts, one of which (called target lift) is situated in the vacuum inside the target chamber and another (that in fact is motor) outside.

A.6. Deactivation

When the work is over, the user pushes the end button. With this the deactivation frame starts. The according LabView scheme is shown in fig. 21. First

the program sends the deactivation command to IXE and then it closes the connection between PC and IXE.
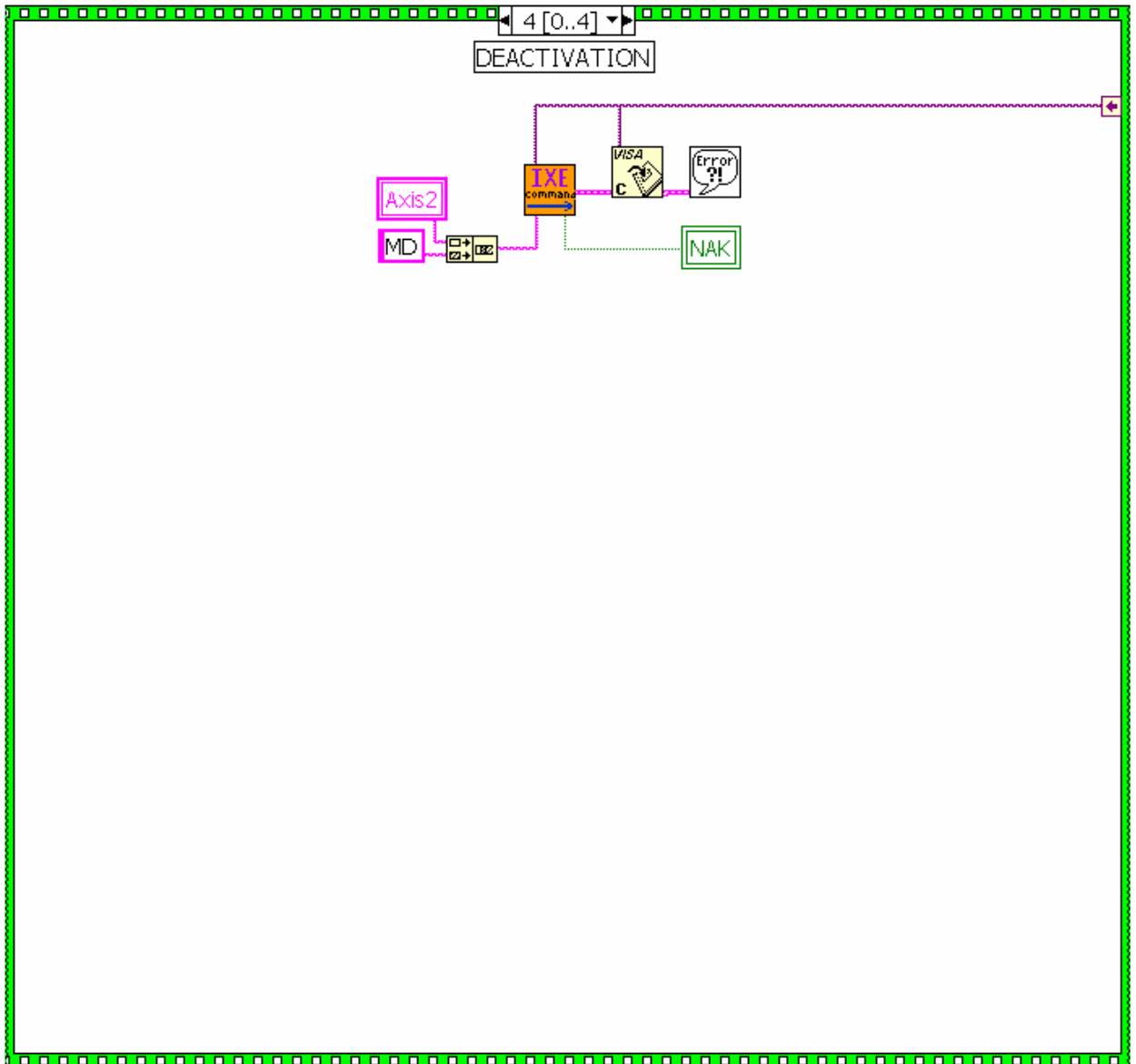

Fig. 21: Deactivation frame.

B. ASCII table

Dec	Hx	Oct	Char		Dec	Hx	Oct	Html	Chr	Dec	Hx	Oct	Html	Chr	Dec	Hx	Oct	Html	Chr
0	0	000	NUL	(null)	32	20	040	 	Space	64	40	100	@	@	96	60	140	`	`
1	1	001	SOH	(start of heading)	33	21	041	!	!	65	41	101	A	A	97	61	141	a	a
2	2	002	STX	(start of text)	34	22	042	"	"	66	42	102	B	B	98	62	142	b	b
3	3	003	ETX	(end of text)	35	23	043	#	#	67	43	103	C	C	99	63	143	c	c
4	4	004	EOT	(end of transmission)	36	24	044	$	$	68	44	104	D	D	100	64	144	d	d
5	5	005	ENQ	(enquiry)	37	25	045	%	%	69	45	105	E	E	101	65	145	e	e
6	6	006	ACK	(acknowledge)	38	26	046	&	&	70	46	106	F	F	102	66	146	f	f
7	7	007	BEL	(bell)	39	27	047	'	'	71	47	107	G	G	103	67	147	g	g
8	8	010	BS	(backspace)	40	28	050	(	(	72	48	110	H	H	104	68	150	h	h
9	9	011	TAB	(horizontal tab)	41	29	051	)	)	73	49	111	I	I	105	69	151	i	i
10	A	012	LF	(NL line feed, new line)	42	2A	052	*	*	74	4A	112	J	J	106	6A	152	j	j
11	B	013	VT	(vertical tab)	43	2B	053	+	+	75	4B	113	K	K	107	6B	153	k	k
12	C	014	FF	(NP form feed, new page)	44	2C	054	,	,	76	4C	114	L	L	108	6C	154	l	l
13	D	015	CR	(carriage return)	45	2D	055	-	-	77	4D	115	M	M	109	6D	155	m	m
14	E	016	SO	(shift out)	46	2E	056	.	.	78	4E	116	N	N	110	6E	156	n	n
15	F	017	SI	(shift in)	47	2F	057	/	/	79	4F	117	O	O	111	6F	157	o	o
16	10	020	DLE	(data link escape)	48	30	060	0	0	80	50	120	P	P	112	70	160	p	p
17	11	021	DC1	(device control 1)	49	31	061	1	1	81	51	121	Q	Q	113	71	161	q	q
18	12	022	DC2	(device control 2)	50	32	062	2	2	82	52	122	R	R	114	72	162	r	r
19	13	023	DC3	(device control 3)	51	33	063	3	3	83	53	123	S	S	115	73	163	s	s
20	14	024	DC4	(device control 4)	52	34	064	4	4	84	54	124	T	T	116	74	164	t	t
21	15	025	NAK	(negative acknowledge)	53	35	065	5	5	85	55	125	U	U	117	75	165	u	u
22	16	026	SYN	(synchronous idle)	54	36	066	6	6	86	56	126	V	V	118	76	166	v	v
23	17	027	ETB	(end of trans. block)	55	37	067	7	7	87	57	127	W	W	119	77	167	w	w
24	18	030	CAN	(cancel)	56	38	070	8	8	88	58	130	X	X	120	78	170	x	x
25	19	031	EM	(end of medium)	57	39	071	9	9	89	59	131	Y	Y	121	79	171	y	y
26	1A	032	SUB	(substitute)	58	3A	072	:	:	90	5A	132	Z	Z	122	7A	172	z	z
27	1B	033	ESC	(escape)	59	3B	073	;	;	91	5B	133	[	[	123	7B	173	{	{
28	1C	034	FS	(file separator)	60	3C	074	<	<	92	5C	134	\	\	124	7C	174	|		
29	1D	035	GS	(group separator)	61	3D	075	=	=	93	5D	135	]	]	125	7D	175	}	}
30	1E	036	RS	(record separator)	62	3E	076	>	>	94	5E	136	^	^	126	7E	176	~	~
31	1F	037	US	(unit separator)	63	3F	077	?	?	95	5F	137	_	_	127	7F	177	&#127;	DEL

Source: www.asciitable.com

References

[1]   A. Richter, Prog. Part. Nucl. Phys. **44** (2000) 3.

[2]   P. von Neumann-Cosel, F. Neumeyer, S. Nishizaki, V.Yu. Ponomarev, C. Rangacharyulu, B. Reitz, A. Richter, G. Schrieder, D.I. Sober, T. Waindzoch, and J. Wambach, Phys. Rev. Lett. **82** (1999) 1105.

[3]   S. Strauch, P. von Neumann-Cosel, C. Rangacharyulu, A. Richter, G. Schrieder, K. Schweda, and J. Wambach, Phys. Rev. Lett. **85** (2000) 2913.

[4]   H.-D. Gräf, H. Miska, E. Spamer, O. Titze, and T. Walcher, Nucl. Instr. Meth. **153** (1978) 9.

[5]   T. Walcher, R. Frey, H.-D. Gräf, E. Spamer, and H. Theissen, Nucl. Instr. Meth. **153** (1978) 17.

[6]   D. Schüll, J. Foh, H.-D. Gräf, H. Miska, R. Schneider, E. Spamer, H. Theissen, O. Titze, and T. Walcher, Nucl. Instr. Meth. **153** (1978) 29.

[7]   J. Foh, R. Frey, R. Schneider, A. Schwierczinski, H. Theissen, and O. Titze, Nucl. Instr. Meth. **153** (1978) 43.

[8]   A. Lenhardt, Diplomarbeit, TU Darmstadt (1999), unpublished.

[9]   P. von Neumann-Cosel and J.N. Ginocchio, Phys. Rev. C **62**, (2000).

[10] A. Richter, Proceedings of the Fifth European Particle Accelerator Conference, ed. S. Meyers et al., (IOP Publishing, Bristol, 1996) 110.

[11] K.T. Hecht and A. Adler, Nucl. Phys. **A137** (1969) 129.

[12] A. Arima, M. Harvey, and K. Shimizu, Phys. Lett. **30B** (1969) 517.

[13] J.N. Ginocchio, Phys. Rev. Lett. **78** (1997) 436; Phys. Rep. **315** (1999) 231.

[14] J.N. Ginocchio and A. Leviatan, Phys. Lett. B **425** (1998) 1.

[15] I.S. Towner, Phys. Rep. **155** (1987) 263.

[16] P. von Neumann-Cosel, Prog. Part. Nucl. Phys. **44** (2000) 49.

[17] B. Reitz, F. Hofmann, P. von Neumann-Cosel, F. Neumeyer, C. Rangacharyulu, A. Richter, G. Schrieder, D. I. Sober, and B. A. Brown, Phys. Rev. Lett. **82** (1999) 291.

[18] J.N. Ginocchio, Phys. Rev. C **59** (1999) 2487.

[19] H. Margenau, Phys. Rev. **58** (1940) 383.

[20] J.C. Hardy and I.S. Towner, Phys. Rev. Lett. **88**, (2002).

[21] C.M. Lederer and V.S. Shirley, Table of Isotopes, 7th Edition (1978).

[22] J. Fuller, W. Fowler, and A. Newman, Astrophys. J. **522** (1982) 718.

[23] M. Carchidi, B.H. Wildenthal, and B.A. Brown, Phys. Rev. C **34**, (1986) 2280.

[24] G. Martínez-Pinedo, A. Poves, E. Caurier, and A.P. Zuker, Phys. Rev. C **53**, (1996) 2602.

[25] Phytron, Manual for Stepper Motor Control Units. Type IXEα-C-MSO, (1999) 35.

Acknowledgements